THERMAL ENHANCEMENT OF BENTONITE-BASED GROUTING MATERIAL BY USING CARBON FIBERS IN GROUND HEAT PUMP SYSTEM

THERMAL ENHANCEMENT OF BENTONITE-BASED GROUTING MATERIAL BY USING CARBON FIBERS IN GROUND HEAT PUMP SYSTEM

By Zhenshun GUAN, M.Eng, B.Eng

A Thesis Submitted to the School of Graduate Studies in Partial Fulfillment of the

requirement for

the Degree of Master of Applied Science

McMaster University MASTER OF APPLIED SCIENCE (2017) Hamilton, Ontario

(Civil Engineering)

TITLE: Thermal Enhancement of Bentonite-based Grouting Material by Using Carbon Fibers in Ground Heat Pump System

AUTHOR: Zhenshun Guan, M.A.Sc Candidate (McMaster University)

SUPERVISOR: Professor Peijun Guo

NUMBER OF PAGES: xiv+113

ABSTRACT

With regard to the global climate changes, green energy and smart resource consumption are highly demanded. There is a great opportunity to make the applications of Ground Heat Pump Systems (GHPS) that take the advantage of green and renewable geothermal resources to save energy consumption, more popular.

In GHPS, the thermal performance of bentonite-based grouting material is a key factor that affects the system efficiency. This research focuses on the enhancement of thermal conductivity and specific heat capacity of bentonite-based grouting material by adding different types and volumetric fractions of carbon fiber. A standard bentonite-sand mix set as a baseline grout was used to assess the additives' effect. Five carbon fiber types supplied by Asbury Carbons, AGM94-0.1mm/3mm/6mm, AGM95-6mm, and AGM99-0.15mm, were investigated in this research. The volumetric fractions of carbon fibers added to the baseline grout ranged from 0.5% to 1.25%.

The laboratory research results demonstrated that the grout thermal conductivity could be increased efficiently by adding higher volumetric percentage and longer carbon fibers. Also, it was found that the greater the fiber aspect ratio, the higher the grout thermal conductivity was. AGM94-6mm carbon fiber had the best enhancement effect on grout thermal performance among the five fibers, although shorter carbon

fibers performed more consistently. AGM95-6mm carbon fiber had a similar performance to AGM94-3mm fiber due to their close aspect ratio and its relative softness. The addition of carbon fibers was not found affect the specific heat capacity of composite grouting material significantly.

A series of on-site bench scale experiments from McClymont & Rak Engineers Inc. was conducted for the potential industrial value of this composite grouting material in GHPS field. Numerical models of this bench scale experiment were also built and simulated using ABAQUS/CAE v6.14. The results were found to be consistent with what is obtained from the field experiments.

ACKNOWLEDGEMENTS

This thesis would not have been possible without the contributions of several people. To all of these people, I wish to express my gratitude.

First and foremost, I wish to thank my thesis supervisor, Dr. Peijun Guo. His expertise and respected reputation in the geotechnical field allowed for the funding of many projects and the opportunity for me to gain knowledge and experience in this geothermal topic. His patient guidance and support on my thesis were instrumental in accomplishing this research.

I also wish to thank Dr. Dieter Stolle who acted as an unofficial co-supervisor along my work of this thesis. His expertise in finite element methods and geo-science were quite valuable in helping me to achieve the academic goals.

My heartfelt appreciation also goes to Mr. Peter Koudys who helped me much in preparing the experimental setup for the tests incorporated in this thesis.

The review and contribution to this thesis by the committee member, Dr. Samir Chidiac are highly appreciated.

Last but not least, I wish to thank my wife, Helen, and my family who give their selfless love and unconditional support to me all the time.

TABLE OF CONTENTS

CHAPTER 1 INTRODUCTION 1

1.1 Background 1

1.2 Research objectives 5

1.3 Thesis outline 6

CHAPTER 2 LITERATURE REVIEW 8

2.1 General development and applications of GHPS 8

2.2 Thermal enhancement methods of GHPS grouting material 11

2.2.1 Grout additives 11

2.2.2 Grout water content 21

2.2.3 Effect of heat exchange pipe 23

2.2.4 Other influencing factors in GHPS 24

2.3 Numerical simulation on GHPS thermal performance 27

2.4 Summary of factors influencing grout thermal performance 30

CHAPTER 3 EXPERIMENTAL STUDIES 32

3.1 Laboratory experiments 32

3.2 Tested experimental materials.. 33

3.3 Grout thermal conductivity tests 38

3.3.1 Testing theory and method..38

3.3.2 Testing setup 41

3.4 Grout specific heat capacity tests... 47

3.4.1 Testing theory and method..47

3.4.2 Testing setup 49

CHAPTER 4 EXPERIMENT RESULTS AND ANALYSIS...55

4.1 Grout thermal conductivity test.. 55

4.1.1 Calibration of thermal needle probe apparatus and baseline grout 56

4.1.2 Effect of carbon fiber additives 59

4.1.3 Non-sand composite grout 66

4.2 Grout specific heat capacity test 69

4.2.1 Standard sapphire calibration..69

4.2.2 Composite grouts test results 73

CHAPTER 5 ON-SITE BENCH SCALE EXPERIMENT AND NUMERICAL SIMULATION 78

5.1 Industrial on-site bench scale experiment 78

5.1.1 MCR bench scale experiment 79

5.1.2 Results of MCR bench scale experiment....86

5.2 Numerical simulation of MCR bench scale experiment 87

5.2.1 ABAQUS heat transfer theory 88

5.2.2 Heat transfer analysis in ABAQUS 91

CHAPTER 6 CONCLUSIONS AND FUTURE WORK....101

6.1 Summary 102

6.1.1 Conclusions from laboratory test results....102

6.1.2 Conclusions from bench scale experiment and numerical simulations ..104

6.2 Future work 104

REFERENCES....107

FIGURES LIST

Figure 1.1 Illustration of Ground Heat Pump System 2

Figure 2.1 Borehole Thermal Energy Storage System in UOIT 10

Figure 2.2 Thermal Conductivity vs Quartz Content for Bentonite-based Mixture 13

Figure 2.3 Thermal Conductivity vs Graphite Content for Bentonite-based Mixture
.... 14

Figure 2.4 Thermal Conductivities for Different Aggregate Types and Proportions
.... 16

Figure 2.5 Thermal Conductivities for Different Additive Types and Volume%..... 18

Figure 2.6 Thermal Conductivity vs Water Content by Börgesson (1994) 22

Figure 2.7 Thermal Conductivity vs Quantity Water by Delaleux et al. (2012)...... 22

Figure 2.8 Increase in Viscosity with Time 25

Figure 2.9 Model of a heterogeneous thermal conductivity field with HGHE....... 28

Figure 2.10 Temperature around underground pipes in different soil conditions. 29

Figure 2.11 Particle orientation (left) and aspect ratio(right) vs ratio of composites thermal conductivity over particle thermal conductivity 30

Figure 3.1 Bentonite powder tested in this research 34

Figure 3.2 Industrial sand tested in this research 35

Figure 3.3 Carbon fibers tested in this research 38

Figure 3.4 Typical record of data 41

Figure 3.4 Grout thermal conductivity testing system 42

Figure 3.5 Experimental apparatus of grout thermal conductivity test 43

Figure 3.6 Experiment procedures of grout thermal conductivity test 46

Figure 3.7 Illustration of sample measurement points in a PVC container 47

Figure 3.8 Typical heat flow curves for specific heat capacity calculation 48

Figure 3.9 Experimental apparatus of grout specific heat test 50

Figure 3.10 Brief laboratory steps of grout specific heat capacity test 52

Figure 4.1 Typical testing result in T-In(t) plane.. 57

Figure 4.2 Grout thermal conductivities comparison 59

Figure 4.3 Influence of carbon fiber volumetric fraction on grout thermal

conductivity for different fiber types... 62

Figure 4.4 Mean values of fiber-added grout thermal conductivity at different fiber volumetric fractions 63

Figure 4.5 Mean values of carbon fiber-added grout thermal conductivity with past research laboratory results from Tiedje and Guo (2013)............................ 64

Figure 4.6 Influence of carbon fiber length and aspect ratio on grout thermal conductivity 65

Figure 4.7 Heat flow curve of standard sapphire sample.................................... 70

Figure 4.8 Summary of composite grout specific heat capacity 75

Figure 4.9 Effect of fiber type and volumetric content on grout specific heat capacity.. 77

Figure 5.1 MCR bench scale experiment.. 78

Figure 5.2 Bench scale test setup 81

Figure 5.3 VERSAPROFILES GeoPerformX pipe... 82

Figure 5.4 Temperature sensors layout (Plane) 83

Figure 5.5 Bench scale test schematic 85

Figure 5.6 Measured temperature distribution of bench scale tests 87

Figure 5.7 Illustration of axisymmetric tank model 93

Figure 5.8 Axisymmetric finite element mesh 94

Figure 5.9 Simulated temperature distribution 95

Figure 5.10 Measured and simulated temperature distribution comparison 97

Figure 5.11 Effect of grout thermal conductivity on simulated temperature distribution 98

Figure 5.12 Effect of sand porosity on simulated temperature distribution 100

TABLES LIST

Table 2.1 Summary of factors influencing grout thermal conductivity 31

Table 3.1 Typical properties of Barotherm Gold 34

Table 3.2 Carbon fibers used for grout thermal enhancement 36

Table 3.3 Components volumetric percentages (%) of testing composite grout ... 44

Table 3.4 Mass of tested samples and Tzero aluminum hermetic containers 53

Table 4.1 Calibration by measuring standard glycerol thermal conductivity 56

Table 4.2 Measurements of composite grout thermal conductivity 58

Table 4.3 Mean values of grout thermal conductivity, W/(m*K) 62

Table 4.4 Non-sand grout materials volumetric fractions (%) 67

Table 4.5 Mean thermal conductivity of non-sand grout and baseline (W/m·K) .. 68

Table 4.6 Summary of DSC calibration test result 72

Table 4.7 Summary of specific heat capacity test results 74

Table 5.1 Material properties (input parameters) 92

Table 5.2 Measured and simulated temperatures at middle height of tank 96

Table 5.3 Effect of applying vacuum on grout thermal conductivity 97

Table 5.4 Simulated temperatures for different grout thermal conductivities...... 98

Table 5.5 Thermal conductivity of quartz sand at different porosities 99

Table 5.6 Temperatures at outside edge of aluminum pipe............................... 101

CHAPTER 1 INTRODUCTION

1.1 Background

Nowadays, energy consumption is getting higher and higher with industrial development. Coal and oil are the top two energy resources for most countries worldwide. According to the research on fossil fuel carbon dioxide emissions by Columbia University (2015), coal and oil contribute more than 80% of the global cumulative total fossil fuel CO_2 emissions in last two and half centuries, 47.5% and 37.2% respectively. The global average surface temperature in 2015 was the warmest on record and reached the symbolic and significant milestone of 1° Celsius above the pre-industrial era by the World Meteorological Organization. This is attributed to a combination of a strong El Niño and human-induced global warming. Based on the report of Natural Resources Defense Council, global warming could cause serious problems such as global sea level rise, extreme hot and dry weather patterns, severe damage on human health and wildlife living ecosystem.

Under such circumstances, the use of green energy, such as solar power, wind power and hydro power, is an irresistible trend. Ground heat pump system (GHPS) has been a rising star. A GHPS is a central heating and/or cooling system that transfers heat to or from the ground. Usually, the main three components of the system are a heat pump equipment, ground loop/borehole/pond, and grouting material as shown in Figure 1.1.

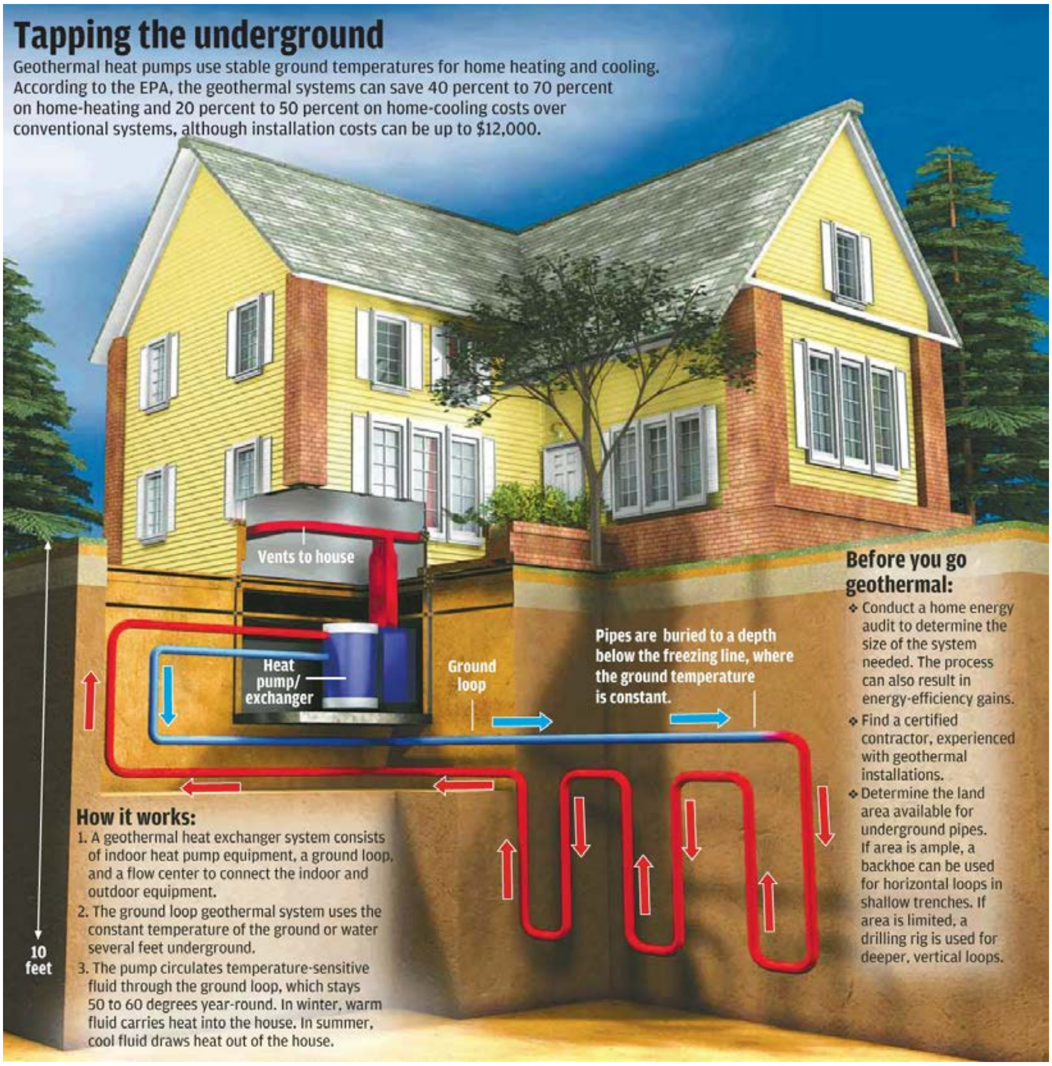

Figure 1.1 Illustration of Ground Heat Pump System
(https://researchhvac.wordpress.com/primary-hvac-systems/geothermal-heat-exchanger/)

GHPS takes advantage of the relatively constant ground temperature. The pump circulates fluid (e.g. water) through a ground loop, which stays at almost constant temperature year-round. During the winter, warm fluid carries heat into the building; while in the summer, the cooler fluid draws heat out of building, which is stored in the ground. The practical usage of ground heat pump system as an efficient way to meet building heating and cooling energy requirements has significantly increased in recent years. According to the Canadian Geothermal Coalition's (2010) finding, from 2005 to 2009 the market for these heat pumps has expanded approximately 44% per year in Canada. This substantial market growth has been attributed to the significantly more competitive economic with regard to operating and maintenance aspects of GHPS when compared with conventional heating and cooling systems.

Based on the Ground-Source Heat Pump Project Analysis chapter from CANMET Energy Technology Centre (CETC) (2004), 46% of the total solar energy absorbed by the earth and stored in thee soil as a thermal reservoir. In contrast to many other sources of heating and cooling energy which need to be transported over long distances, earth energy is available on-site, and in massive quantities. The GHPS model is also validated to be more than adequate at the feasibility stage of implementation by CETC.

Among the three components of GHPS, the grouting material plays the most important role on the thermal performance of the system provided a compatible soil surrounding the system. Both Delaleux (2012) and Desmedt (2012) point out that GHPS performance is strongly influenced by the thermal properties of the ground formation and grouting material, especially the thermal conductivity of the grout. The higher the conductivity of the grout, the more heat that can be transferred per unit length of borehole. Kavanaugh and Allan (1999) note that the American Brookhaven National Laboratory and Alabama University begin cooperation to seek optimal performance of closed-loop borehole heat exchangers, which depends significantly on the thermal properties of the backfill or grouting material in the annular region between tubes and the outer borehole wall. Delaleux show an overall cost reduction of 30% for a same delivered thermal power could be achieved by making use of thermally enhanced grouting material when compared with a non-enhanced one. Desmedt and Van Beal (2012) indicate that the use of standard bentonite grout instead of thermally improves bentonite grout, increased the loop length by 24%.

The use of grouting material with high thermal conductivity increases the heat exchange rate for the same borehole length, which implies that higher thermal conductivity of the grout brings a lower cost on borehole construction and fluid-circulating tube. Means to increase the thermal conductivity of grouting material is important for enhanced performance and more economical ground heat pump systems. This is the core of the relevant research in this field presented in the literature review of Chapter 2.

The application of GHPS can be found in many homes and businesses buildings across the province of Ontario. In fact, Ontario has dominated when it comes to deploying geo-thermal systems, according to a national report from the Canadian GeoExchange Coalition (2012), a non-profit organization representing the industry. Changes to the province's building code in 2011 that require buildings to be 25% more efficient has further boosted interest in this technology. Even at McMaster University, installation of GHPS has been installed for Gerald Hatch Centre.

1.2 Research objectives

The objective of this research is to study the effect of carbon fibers as an additive on the thermal performance of bentonite-based grout and to determine the optimal proportions of each grout component. The focus is placed on factors that affect the bentonite-based grout thermal properties, especially the thermal conductivity, and to build numerical models that are capable of predicting the heat pump system thermal performance observed in the laboratory.

The findings are expected to provide guidance for using of carbon fibers as part of a high thermal performance bentonite-based grouting material in GHPS.

To achieve the above goals, the following tasks have been carried out:

- Determine the effect of different add-in materials on bentonite-based grout components on grout thermal conductivity;
- Determine the effect of carbon fiber volumetric fraction, fiber length, aspect ratio, and carbon content on grout thermal conductivity and specific heat capacity;
- Compare the composite grout achieved from laboratory tests with current available industrial products on market;
- Build numerical models to predict thermal performance of GHPS with carbon fiber enhanced bentonite-based grout and compare the simulation outcomes with laboratory results.

1.3 Thesis outline

This thesis consists of six chapters including this introduction as Chapter 1.

Chapter 2 presents a literature review focusing on research of the last two decades on diverse methods to thermally enhance GHPS grouting materials including applications of using special additives such as graphite and carbon fibers. The factors that possibly affect the thermal performance of GHPS, especially the thermal conductivity of grouting/backfill material in practical industry are discussed.

Chapter 3 presents details of the experimental work that involves both thermal conductivity and specific heat capacity tests of bentonite-based grouting material containing carbon fibers. The thermal performance of GHPS grout enhanced by using different types of carbon fibers is investigated.

The analysis of laboratory results of various thermal property tests in which different types of carbon fibers were investigated is part of Chapter 4. In this chapter, the effects of various factors and possible reasons are discussed. The comparison between the composite grout achieved in laboratory test and available industrial products on the market is also made.

In Chapter 5, a numerical model is built for simulating the thermal performance of GHPS based on laboratory test outcomes and the simulated results are used to compare with the on-site experiment results from an industrial company.

Last but not least, Chapter 6 summarizes the major findings of this research and gives an outlook on future research activities.

CHAPTER 2 LITERATURE REVIEW

2.1 General development and applications of GHPS

The development of ground-source heat pump systems dates to 1912 when the first patent using a ground loop was recorded in Switzerland. However, it was not until the 1970's that GHPS gained significant market acceptance. The first commercial GHPS were designed as groundwater-type systems for residential use. By the mid 1980's, advances in heat pump efficiencies and operating ranges, combined with better materials for ground loops, allowed for ground-coupled earth connections. At about the same time, commercial and institutional applications became more common.

As pointed out in Ground-Source Heat Pump Project Analysis by the Minister of Natural Resources Canada (2005), markets for GSHPs tend to be particularly strong when climate, energy prices and the nature of the project are favourable. A climate requiring both heating and cooling is preferable to one that requires just one or the other. Two separate conventional systems may be required, each dedicated to only one task, either heating or cooling. Since the same GSHP system can provide both heating and cooling. It tends to decrease the capital cost of the green technology, making the GSHP a more attractive option. Furthermore, since it is operating year-round, the

GSHP system can generate larger energy savings, rather than an air-conditioning unit which only operates in summer and an oil furnace which only operates in winter.

Sanner (2003) states that for each kWh of heating/cooling output, 0.22-0.35kWh electricity is required for a typical borehole heat exchanger (BHE) or vertical ground heat exchanger in Europe. This required energy is 30%-50% less than the seasonal power consumption of air-to-air heat pumps that use the atmosphere as a heat source/sink. BHE or vertical ground heat exchangers show better performance and energy efficiency than horizontal ground heat exchangers. Sanner emphasizes that use of thermally enhanced grouting material is an effective way to reduce BHE thermal resistance. In addition, the use of spacers in order to keep individual fluid-circulating pipes apart and bring them close to the borehole wall is another option.

Spitler and Qing (2006) report that approximately 20,000 new BHEs are installed each year in North America. Based on the findings from American Brookhaven National Laboratory and Alabama University, optimal performance of closed-loop ground heat exchangers in the backfill of BHEs depends on the thermal properties of the backfill/grout in the annular region between pipes and the outer bore wall. They indicate that the grouts, which are enhanced with low-cost additives have thermal conductivities up to four times larger than conventional grouts. The huge market potential of this renewable and environmental friendly energy system outside Europe and North America was also analyzed.

Dincer (2004) carried out the largest scale borehole thermal energy storage project in Canada, which is established at University of Ontario Institute of Technology (UOIT), as shown in Figure 2.1. The project, which has 384 boreholes, each 213 meters deep, provides the basis for a highly efficient and environmental friendly heating/cooling system, capable of regulating eight university buildings.

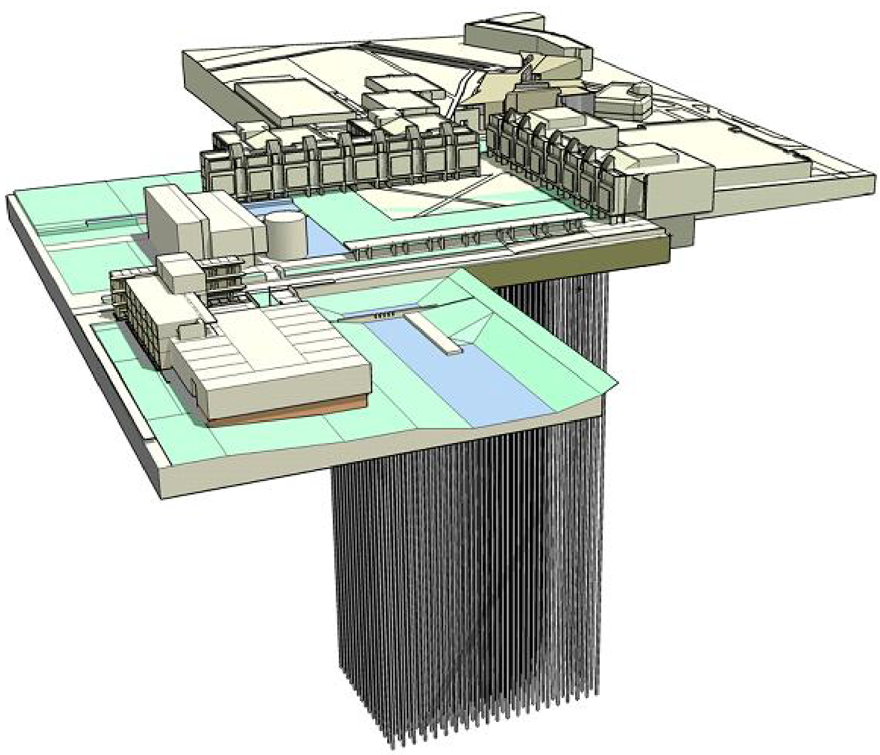

Figure 2.1 Borehole Thermal Energy Storage System in UOIT
(http://www.engineering.uoit.ca/research/research-facilities/)

2.2 Thermal enhancement methods of GHPS grouting material

According to Delaleux (2012) and various related research, including that mentioned in 2.1, the thermal properties, especially thermal conductivity of grout material, mainly affect the GHPS thermal performance, which determines the thermal efficiency of the whole system. Therefore, how to effectively increase the grout thermal conductivity and/or enhance the system thermal performance becomes an important challenge of the industry. The main methods are introduced below.

2.2.1 Grout additives

Based on Leong and his colleagues (2014), there is a natural spread in the thermal conductivity of various bentonite materials. The average value of thermal conductivity is approximately 1.2 W/m·K and the lower boundary can be as low as 0.6 W/m·K. To obtain a grout with high thermal conductivity, it is widely accepted by industry that high thermal conductivity additives must be used.

Quartz or silica sand is one of the most common additives used to enhance the thermal conductivity of bentonite grouts. A number of studies have consistently shown that the addition of quartz/silica sand enhances the thermal conductivity of bentonite alone. However, the degree to which the thermal conductivity is enhanced is relatively small, according to Leong et al. (2014). They state that the principal reasons for adding sand to bentonite are to improve the mechanical stability and, for economic reasons, to reduce the amount of bentonite being used. Besides, the addition of sand to bentonite grout tends to significantly increase the grout hydraulic conductivity and lower the swelling pressure which are to be avoided in most cases. High percentage of sand tends to increase the viscosity and to reduce the workability, flowability and pumpability of the grout. The increase of thermal conductivity by adding sand without sacrificing workability or pumpability of the grout is limited.

Jobmann and Buntebarth (2009) investigated the effect of adding quartz to bentonite on the thermal conductivity of the mixture. They found, increasing quartz content to 50% only increases a mixture's thermal conductivity by 55% under 20°C (shown in Figure 2.2). Even with the addition of significant quantities of sand/quartz, the increase in the thermal conductivity of the resulting bentonite mixture is still small. Research conducted by Remund and Lund (1993) reveal similar findings.

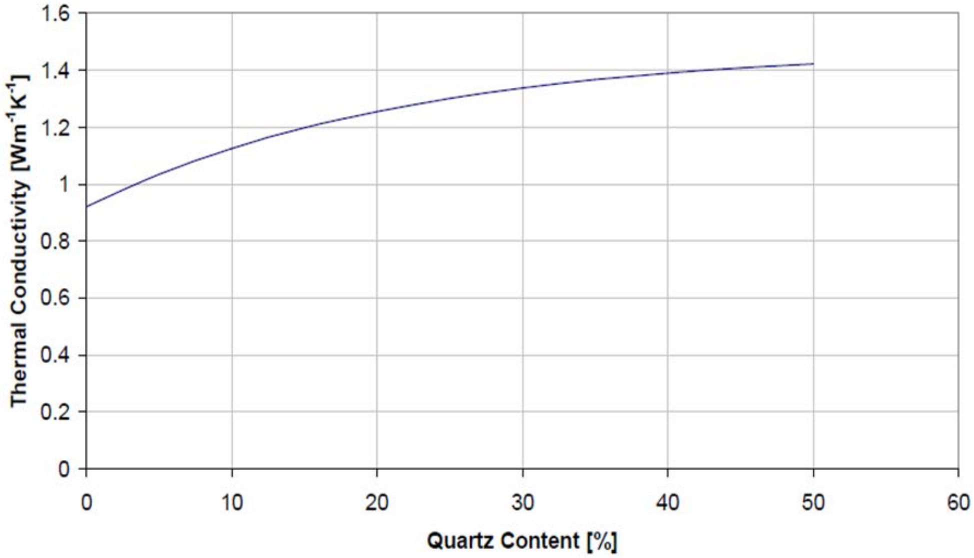

Figure 2.2 Thermal Conductivity vs Quartz Content for Bentonite-based Mixture

Jobmann and Buntebarth (2009) also show that the thermal conductivity of a bentonite/graphite mixture increases with increasing graphite content. An empirical relation between the thermal conductivity of the bentonite mixture and graphite content is shown in Figure 2.3. Based on their study, using a reasonable graphite content around 15%, the thermal conductivity of this graphite/bentonite mixture can easily be higher than 2.0 W/m · K.

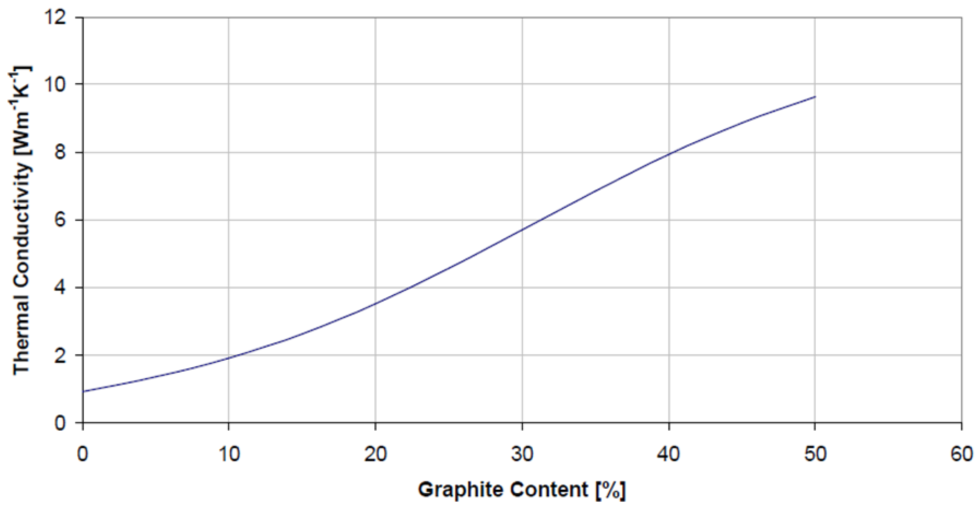

Figure 2.3 Thermal Conductivity vs Graphite Content for Bentonite-based Mixture

Delaleux and his teammates (2012) investigated the use of graphite flakes, expanded natural graphite (ENG), and compressed expanded natural graphite (CENG) for increasing the thermal conductivity of bentonite/graphite composite grout in BHEs. They find high thermal conductivity intensifications for low graphite contents using CENG: up to 5.0 W/m·K at only 5% graphite by weight. This effective grout conductivity leads to an increase in overall heat transfer of 50% for a reduced and consequently realistic graphite load.

Although graphite shows an exciting effect on grout thermal conductivity enhancement, there are still some disadvantages of this material. As pointed out by Leong (2014), some waste management programmers have rejected the use of graphite because of possible deleterious effects on buffer/grout performance. For example, ANDRA has rejected the use of graphite in buffer/grout materials, because of the effect it could have on steel corrosion. France is also no longer considering the use of graphite as an additive to buffer/grout material. Moreover, unlike bentonite, where thermal conductivity is not sensitive to temperature, the thermal conductivity of graphite decreases as temperature increases.

Research on thermally enhanced grout other than bentonite-based type has high reference value as well. Trevino and colleagues (2013) investigated some natural and recycled types of aggregates including limestone sand (L), electric arc furnace slag sand (EAF), construction and demolition waste sand (CDW), and compared the thermal conductivities between cement-based grout by adding these sands and the same grout with normal Silica sand (S) in BHEs. They conclude that the use of any of these aggregates improves the grout thermal conductivity, independently of the proportion used. Limestone sand, silica sand and electric arc furnace slag enhance the thermal conductivity of the grout with the increase of their volumetric fraction. Meanwhile, no satisfactory results are obtained for construction and demolition waste-based mixes because of their high-water requirement. Figure 2.4 shows Trevino and colleagues (2013) research findings. It is clearly illustrated that the recycled aggregates are less effective on increasing grout thermal conductivity compared with silica sand. However, sand has been negatively evaluated by considering increasing permeability and damaging pump equipment.

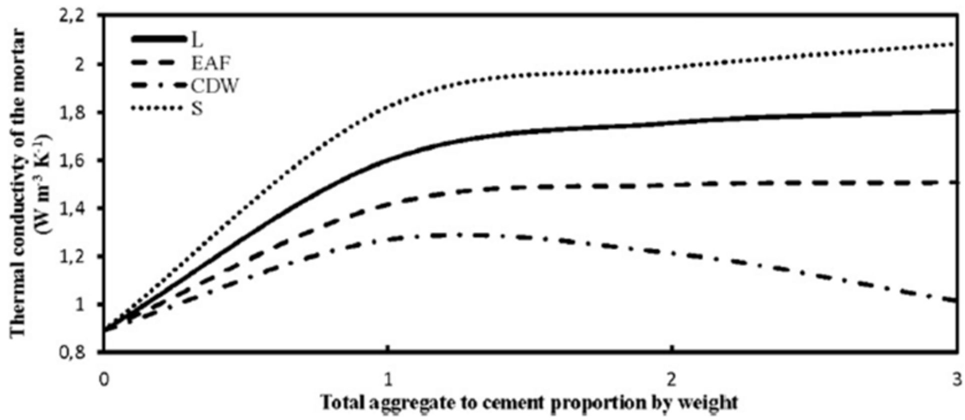

Figure 2.4 Thermal Conductivities for Different Aggregate Types and Proportions

Alrtimi and teammates (2013) conducted a research on the thermal enhancement of PFA (Pulverized Fuel Ash) based grout in geothermal heat exchanges. The effects of fine sand, coarse sand, ground glass, and fluorspars were investigated under both dry and saturated PFA-based grout conditions. They obtained poor enhancement of thermal conductivity using fine sand or medium ground glass, having only a maximum value of 1.15 W/m·K at saturation. Use of coarse or mixed ground glass gave a maximum value of 1.39 W/m·K. The highest values were achieved when using fluorspar or coarse sand where the thermal conductivity reached 2.88 and 2.47 W/m·K, respectively, at 80% by weight. It was also observed that the combination of fluorspar with coarse ground glass resulted in relatively high thermal conductivity for both dry and saturated conditions. However, neither fluorspar nor coarse aggregates could provide enough low grout permeability due to their particle sizes.

Compared with all above mentioned additive materials, carbon fiber has many advantages to be chosen as the right additive for grouting material in GHPS. Its favored properties include high thermal conductivity, high tensile strength and rigidity, corrosion resistance, fatigue resistance, fire resistance, low coefficient of thermal expansion, non-toxicity, biologically inert, and self lubricating. According to Huang (2009), a carbon fiber's coefficient of thermal conductivity is in the range of 21-125 W/m·K, which is close to that of metals. For the case of high modulus mesophase-pitch carbon fibers, thermal conductivity can be more than 500 W/m·K at room temperature.

Tiedje and Guo (2014) report on a research addressing bentonite-based grout thermal conductivity. They use different fiber-length carbon fibers. Fibers 0.15mm and 3mm long are investigated and performance is compared with that of flake graphite and compressed expanded natural graphite (CENG), shown in Figure 2.5. They point out that higher fiber volumetric fraction results in a higher composite grout thermal conductivity. The mean conductivity is increased by approximately 50% compared to that of non-fiber grout at a total carbon fiber volumetric fraction of only

0.68%, which corresponds to 22g of fibers per kilogram of bentonite and sand. They indicate that 3-mm carbon fibers are more effective than either flake graphite or CENG. At a volume fraction of 0.68% the 3-mm fibers are almost twice as effective as either form of graphite. The influence of adding carbon fibre on the viscosity, workability, flowability and pumpability of the grout still needs to be investigated.

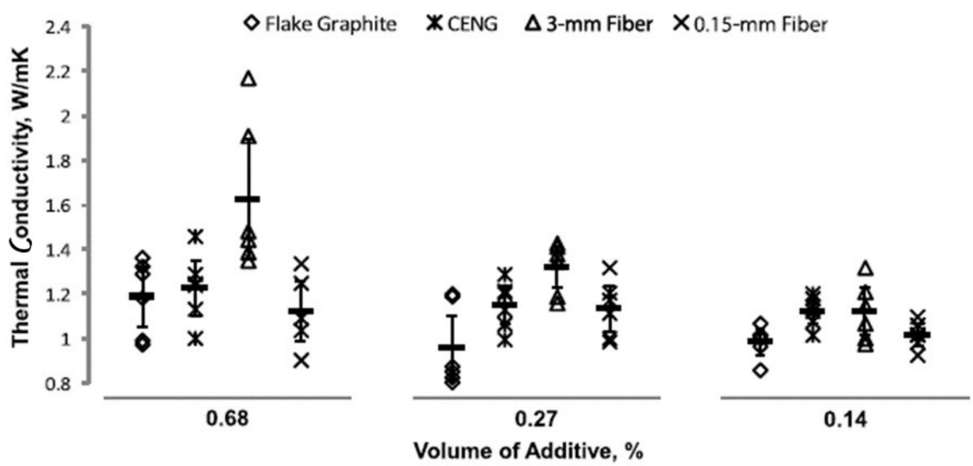

Figure 2.5 Thermal Conductivities for Different Additive Types and Volume%

Back in the past century, Agari and teammates (1991) suggest that longer carbon fibers can provide a higher thermal conductivity. It is attributed to an easier conductive-chain-formation in composite material, assuming carbon fiber composite is quantitatively evaluated to be isotropic.

In addition to the fiber length and volumetric fraction, the fiber aspect ratio affects composite grout thermal conductivity. Demain and Issi (1992) suggest a positive correlation between fiber aspect ratio and grout thermal conductivity. However, they assume that once the aspect ratio becomes greater than 50, it does not significantly increase the composite thermal conductivity any more. What's worth more attention is that they observe that a fiber's thermal conductivity is strongly oriented in a composite leading to highly anisotropic thermal conductivity. Longitudinal thermal conductivity, comparable to that of metal, is achieved in the direction of fibers, while in transverse direction only a small increase is observed.

Tiedje and Guo (2014) apply FEM simulations to demonstrate that the conductivity of composites grout is affected by not only the relative volume and conductivity of the embedded particles, but also their general shape, elongation, and orientation relative to the direction of global heat flow. Generally, when the orientation of fibers is parallel to the global thermal gradient, the thermal conductivity in the direction of the global thermal gradient increases with an increase of aspect ratio, AR; while for fibers perpendicular to the global thermal gradient, the thermal conductivity tends to decrease with increasing AR. This conclusion is consistent with the findings by Demain and Issi (1992).

According to Miller and Rifai (2004), in addition to increasing the thermal conductivity of grout, using fiber as an additive also effectively prevents the development of desiccation cracks, increases soil workability and compaction characteristics, and reduces the hydraulic conductivity of the composite grout. Sanner (2003) also suggests that grouting material should stay somewhat plastic to accommodate thermal dilation of pipes and meet the requirement of good filling and contact to pipes and borehole wall as well as the good plugging of the hole.

Despite carbon fiber having a relatively high thermal conductivity itself, Naito and his colleagues (2011) suggest that grafting carbon nanotubes on carbon fibers could increase the thermal conductivity by another 30% no matter if the carbon fibers are PAN-based or Pitch-based. This research provides the possibility on further increasing the grout thermal conductivity in GHPS to an unreached high level in the future. PAN-based fiber can be polymerized from acrylonitrile by commonly used initiators, such as peroxides and azo compounds, through the addition polymerization process. The process can be either solution polymerization or suspension polymerization. While synthetic Pitch-based fiber is produced by the pyrolysis of synthetic polymers. The composition of a Pitch varies with the source tar and the processing conditions.

2.2.2 Grout water content

Water content is another important factor that affects a grout thermal conductivity. Leong and his colleagues (2014) investigate the correlation between the thermal conductivity of grout mixture and water content or dry density. The thermal conductivity results measured by Börgesson (1994) show that the difference of thermal conductivity between a dry bentonite and a fully saturated bentonite can be more than a factor of 2, as illustrated in Figure 2.6. Delaleux et al (2012) state that partial drying of the grouts induces a significant decrease in thermal conductivity in the range of 1 W/m·K for 10% weight of water content reduction, as shown in Figure 2.7. The verification by Jobmann and Buntebarth (2009) for a positive correlation between the thermal conductivity of bentonite with 15% weight graphite and its dry density also supports the effect of water content on the grout thermal conductivity.

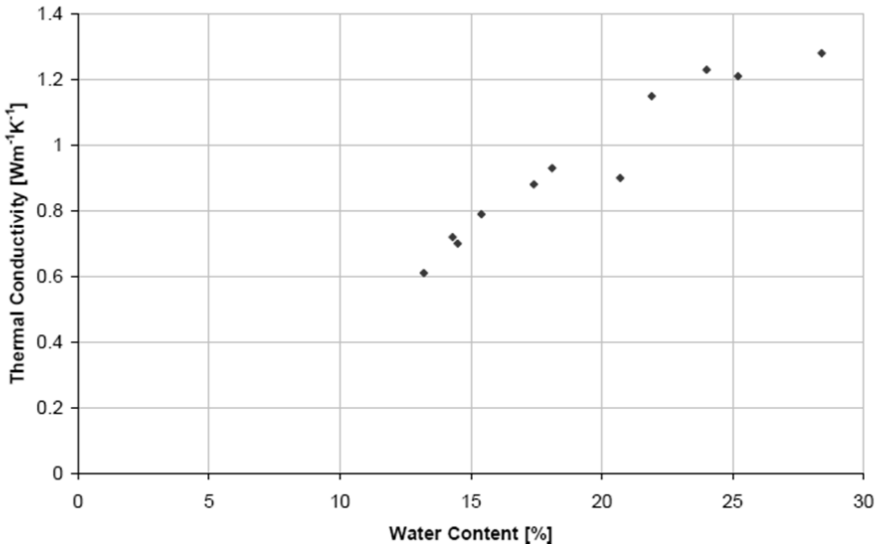

Figure 2.6 Thermal Conductivity vs Water Content by Börgesson (1994)

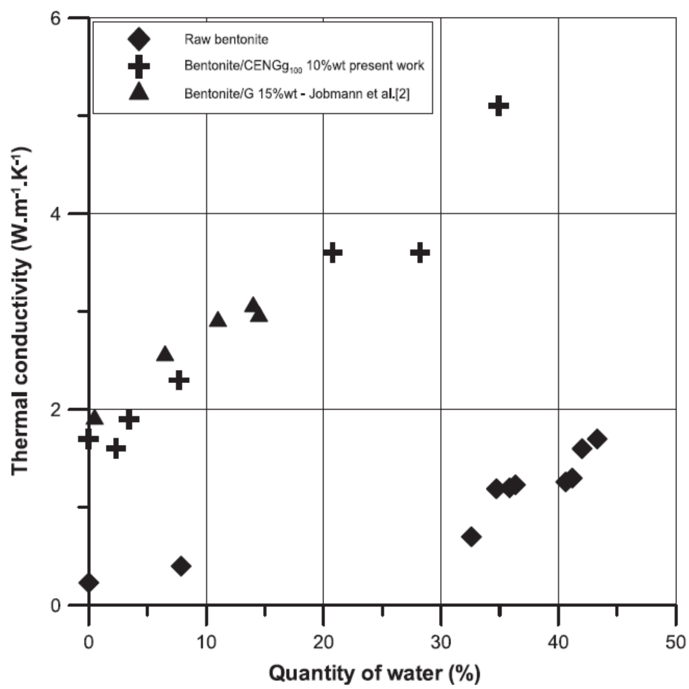

Figure 2.7 Thermal Conductivity vs Quantity Water by Delaleux et al. (2012)

2.2.3 Effect of heat exchange pipe

Simms and coworkers (2013) examine the effect of space between heat exchange pipes in horizontal ground heat exchangers (HGHE). They propose that 50cm is the current best practice of targeting pipe spacing, which should be continued. Narrowing the pipe spacing clearly makes the HGHE more sensitive to soil heterogeneity and strengthen the heat transfer pathways between pipes, which is observed to reduce the efficiency of such systems.

Sanner (2003) suggests that use of spacers to keep the individual pipes apart and bring them closer to the borehole wall is an effective way to enhance the BHE thermal performance when grout thermal conductivity can not be increased. For a 15cm diameter borehole, using 8cm shank spacing increases the thermal performance of BHE by 40% compared with that of using only 4cm shank spacing.

In addition to between-pipe space, pipe type and material also matter. Desmedt and colleagues (2012) carried out an experimental investigation on 11 BHE types and grouting materials in Belgium. They found that the double-U pipe gives the best-performing BHE, followed by the single-U pipe and the coaxial, on the borehole resistance.

2.2.4 Other influencing factors in GHPS

Grout viscosity

Lee and his colleagues (2009) conducted a series of experiments on thermally-enhanced bentonite grouts in South Korea. They find that both the thermal conductivity and the viscosity of the bentonite grouts increase with the content of silica sand and graphite. Figure 2.8(a) and 2.8(b) show a significant increase in viscosity with time for 6 hours. The rate of viscosity increase becomes greater when the amount of additive mixed in the grout increases. The borehole filling and contact are adversely affected by higher grout viscosity since low-thermal-conductivity air can be entrapped, thereby weakening the system’s thermal performance. Lee (2009) indicates that care must be taken not to delay significantly grout pumping operation after preparing the composite grout in the field.

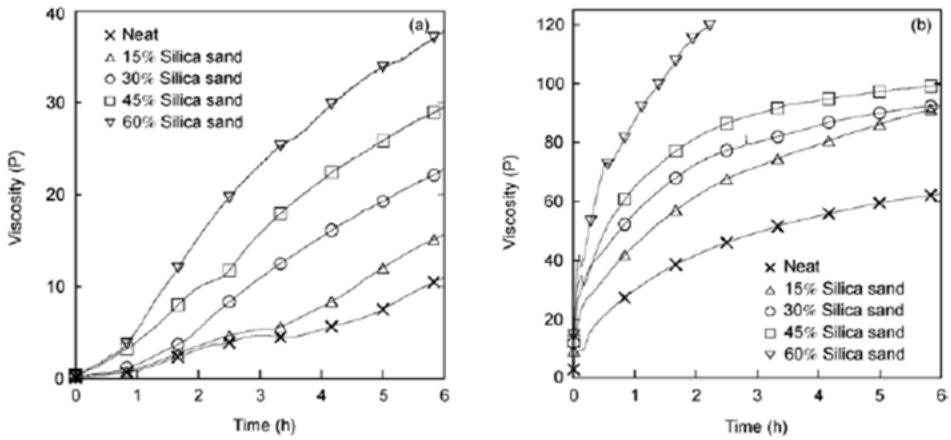

(a) 20% bentonite + silica sand

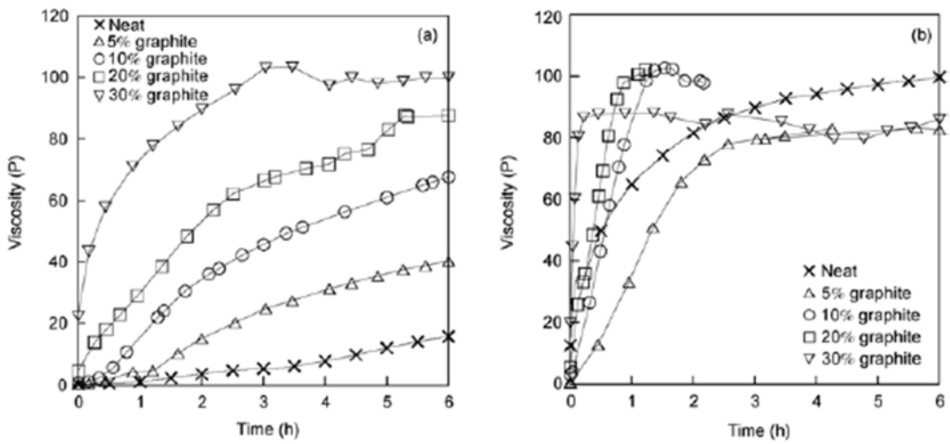

(b) 20% bentonite + graphite

Figure 2.8 Increase in Viscosity with Time

Grout temperature

For some materials, the value of thermal conductivity varies with temperature. Based on Leong et al (2014), the thermal conductivity of both bentonite grout and bentonite-sand mixture increases when temperature rises. However, the thermal conductivity of graphite decreases as temperature increases. Under in-situ condition, Mands and Sanner (2001) observe that a changing of thermal conductivity due to temperature induced moisture migration in water-saturated sediments.

Particle shape and size of grout additive

Fujii and coworkers (2011) carry out in-situ thermal response tests and laboratory tests to investigate the applicability of large size gravels as filling material of GHPS. They propose that using large grain size gravels can effectively increase a grout's thermal conductivity compared with that of using small grain size material such as silica sand. However, large grain size material has two main disadvantages; namely, high permeability and poor pumpability. Large grain sizes can cause damage to pump equipment during construction. Large grained additives lead to a high pressure that causes pipes to break when boreholes are designed as deep as 200 meters for BHE systems.

Soil heterogeneity

To simplify problems, soil is considered isotropic and homogeneous in most GHPS projects. But in reality, natural soil is often anisotropic and heterogeneous. According to Simms (2013) and colleagues' findings, the impact of soil heterogeneity is within the boundaries of uncertainty in mean thermal conductivity. They conclude that the effect of soil heterogeneity is found to be minimal relative to the uncertainty of the mean soil thermal conductivity, supporting the continued use of the assumption of homogeneity when modelling and designing ground heat pump systems.

2.3 Numerical simulation on GHPS thermal performance

Numerical models of GHPS provide necessary technical support for designers to predict system thermal performance for practical conditions which helps to save investment and increases efficiency at the research stage.

Simms et al (2013) evaluate the effect of heterogeneity of soil in horizontal ground heat exchangers (HGHE) by modeling the system using a finite element code, shown in Figure 2.9. Based on their FEM simulations, heat transfer pathways between pipes are observed to reduce the efficiency of such systems. High thermal conductivity soil beneath and to the sides of the ground heat exchangers increases the effective volume of the trench and improves the loop performance. It is also suggested that the current best practice of targeting 50cm pipe spacing should be continued. The heterogeneity is a less important design factor than the effective mean thermal properties and thus is assumed to have no practical impact on performance.

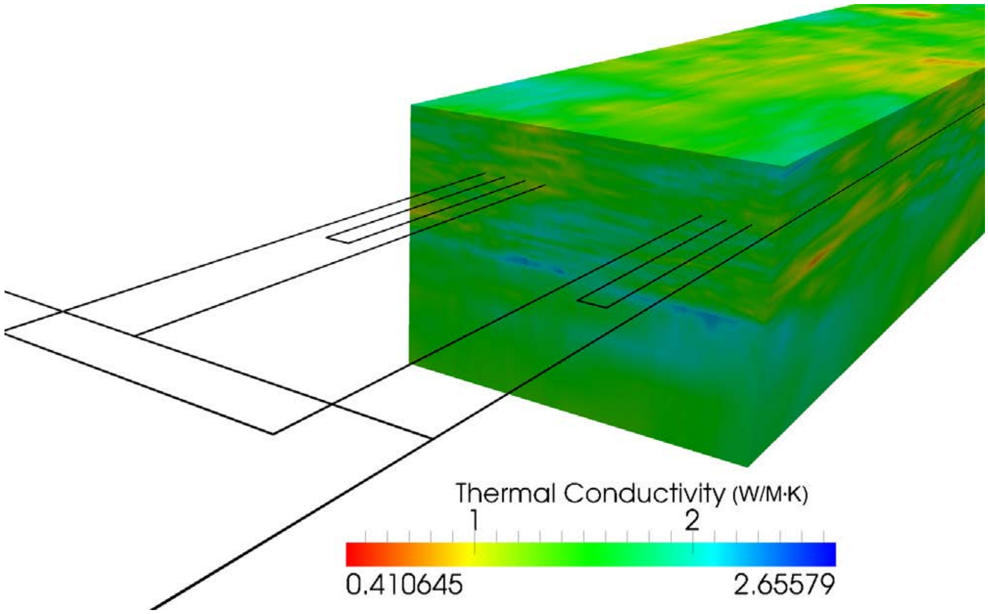

Figure 2.9 Model of a heterogeneous thermal conductivity field with HGHE

Zheng and his colleagues (2011) build a model in Matlab to study the thermal performance of vertical U-tube ground heat exchangers. They discover that when the thermal conductivity increases, the thermal effective radius of the pipe becomes larger and the scope of the impact for the soil becomes broader as shown in Figure 2.10. High thermal conductivity materials can exchange heat well through the pipe, while the heat is spread out and then the temperature increment near the pipe is also lowered. For greater heat flow and less probability of heat short-circuit phenomenon, it is advised to keep an appropriate center distance, 10-20cm, of the tube legs in engineering practice. The design of vertical pipe groups should guarantee at least 3m between drilling space to decrease the effect of heat transfer between the exchanger and the soil.

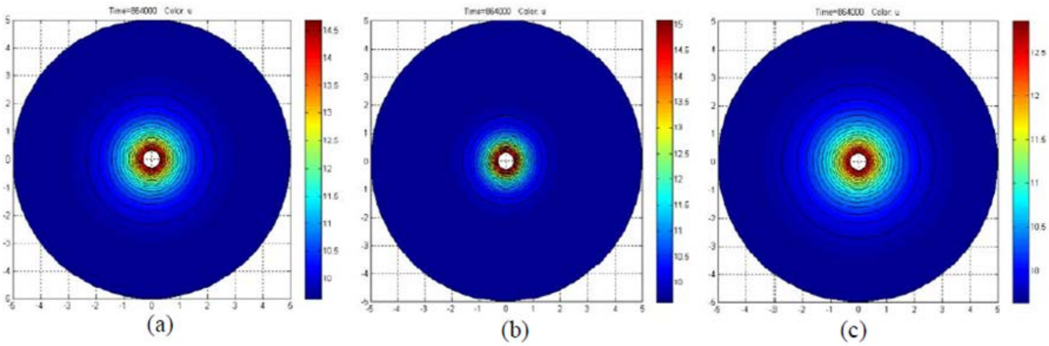

Figure 2.10 Temperature around underground pipes in different soil conditions (Grout thermal conductivities order: (b)<(a)<(c).)

Tiedje and Guo (2014) examine through a series of FEM simulations the correlations between the thermal conductivity of two-phase, discrete particle composites and particle geometry and volumetric fraction. These simulations demonstrate that the conductivity of such composites is influenced by not only the relative volume and conductivity of the embedded particles, but also their general shape, elongation, and orientation relative to the direction of global heat flow. In particular when the orientation of the particle is parallel to the global gradient, the composite conductivity in the direction of the global thermal gradient increases with the aspect ratio, while for particles perpendicular to the global thermal gradient the composite's conductivity tends to decrease with increasing aspect ratio. For composite with one particle type, its homogenized thermal conductivity is positively correlated with ratio of particle's conductivity over matrix conductivity, particle's volumetric fraction, and particle's aspect ratio. The influence of aspect ratio is more pronounced when particle's volume fraction is large.

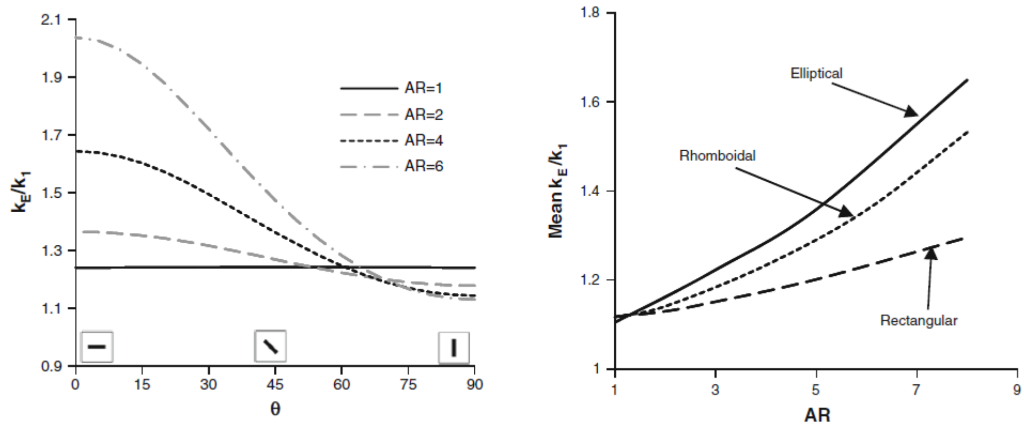

Figure 2.11 Particle orientation (left) and aspect ratio(right) vs ratio of composites thermal conductivity over particle thermal conductivity

2.4 Summary of factors influencing grout thermal performance

Generally speaking, the thermal conductivity of bentonite-based grout is an important factor for a GHPS's thermal performance. For composite bentonite-based grout, the particle's geometry and orientation of additives, such as carbon fibers, graphite, and sand, are very important for the grout thermal conductivity. The additive content is also important.

The summary of factors influencing bentonite-based grout thermal conductivity mentioned previously is presented in Table 2.1.

Table 2.1 Summary of factors influencing grout thermal conductivity

Factor	**Variation**	**Grout Thermal Conductivity**	**Importance**
Water content	increase	increase	high
Additive volumetric%	increase	increase	high
Additive particle geometry (size)	increase	increase	medium high
Additive particle orientation	longitudinal/ transversal	relatively high/low	medium high
Temperature	increase	increase	medium low
Temperature (with graphite)	increase	decrease	medium low
Soil heterogeneity	increase	not obvious	low
Pipe spacing	increase	slightly increase	low

CHAPTER 3 EXPERIMENTAL STUDIES

This chapter describes two laboratory experiments conducted in this study, the experimental materials, devices, and testing procedures.

3.1 Laboratory experiments

To investigate the effect of adding carbon fibers as an additive on the thermal behaviour of composite bentonite-based grout, two series of laboratory tests were conducted: grout thermal conductivity test and grout specific heat capacity test.

The thermal conductivity tests were performed to determine the thermal conductivity of composite bentonite-based grout with five different types of carbon fibers being used at four different volumetric concentrations based on line source theory. For comparison, a baseline mix was developed to approximate the composition of a typical bentonite grout used in engineering practice.

The specific heat capacity tests were carried out to measure the specific heat of these fiber-added composite grouts by using a differential scanning calorimeter.

Both experiments aimed to evaluate the potential of carbon fibers as an additive to improve the thermal performance of composite bentonite-based grout in GHPS. Details of these two experiments are provided in this chapter.

3.2 Tested experimental materials

The experimental materials used to produce composite grout include bentonite powder, industrial sand, carbon fibers and de-aired water.

The bentonite powder was “Barotherm Gold” from Baroid Industrial Drilling Products. This sodium bentonite is an industrial-grade powder marketed for use in vertical ground source heat exchangers. Guidelines are available from the manufacturer for enhancing the thermal conductivity of the grout by blending the bentonite powder with common silica sand, shown in Figure 3.2. Typical properties of the bentonite powder are listed in Table 3.1.

The industrial sand was supplied by the same supplier. This sand is an industrially available, clean, uniformly graded, silica or quartz sand. The coefficient of uniformity, C_U, is 1.0 and the coefficient of curvature, C_C, is 1.8. The mean particle size of the sand, D_{50}, is 0.27mm. The specific gravity was 2.62 obtained from laboratory test. The particle size distribution curve is presented in Figure 3.2.

(a). Bentonite powder - Barotherm Gold from Baroid

Thermal Conductivity (W/m·K)	kg of Sand / 22.7kg bentonite	L. of Water / 22.7kg bentonite	Total Solids (Mass %)	Total Solids (Volume %)
0.69	0	57.9	28.1	13.1
1.19	45.4	57.9	54.0	31.0
1.32	68.0	61.7	59.5	49.6
1.52	90.7	65.5	63.4	54.3
1.73	113.4	69.3	66.3	57.6
1.9	158.8	75.7	70.6	63.2
2.08	181.4	79.5	72.0	64.9

(b). Official recommended grout treatment

Figure 3.1 Bentonite powder tested in this research

Table 3.1 Typical properties of Barotherm Gold

Appearance	Specific gravity	Yield volume range (L./22.7kg)	Grout weight range (kg/L.)	Permeability (cm/s)
Beige/tan powder	2.6	66.7-158.2	1.2-1.8	$<1.0\text{x}10^{-7}$

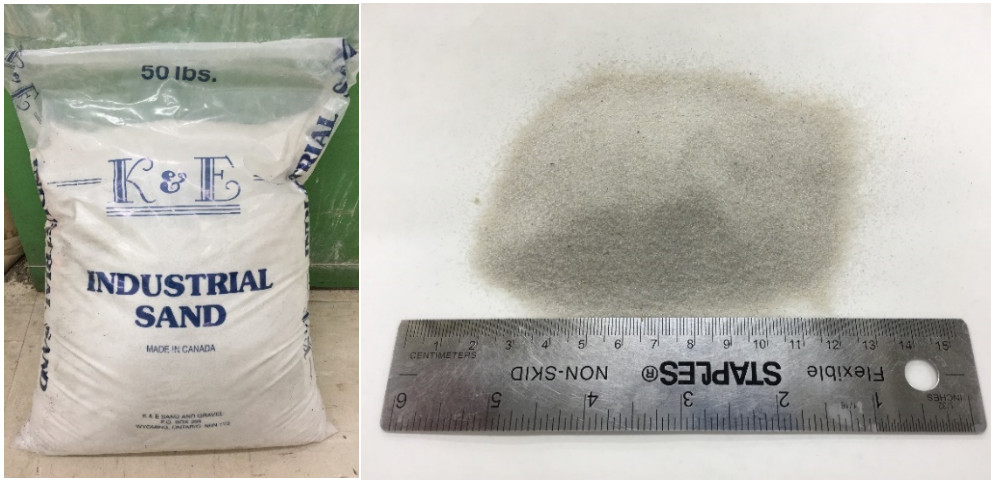

(a). Industrial sand - from Baroid

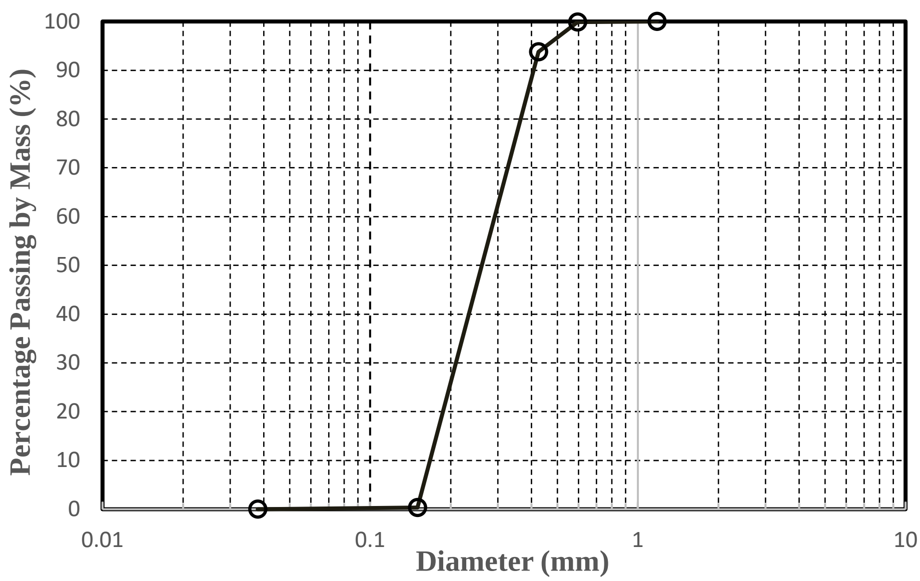

(b). Particle size distribution curve

Figure 3.2 Industrial sand tested in this research

There were five different types of carbon fibers investigated in this research, which had different fiber diameter, from 0.0072mm to 0.0138mm, and different fiber length, ranging from 0.1mm to 6mm. The fiber’s carbon content was no less than 95%.

All fibers were supplied by Asbury Carbons Inc. for material properties consistency. According to the data provided by the supplier, the thermal conductivity of the carbon fibers was **17.1** W/m·K. Table 3.2 summarizes the basic properties of the carbon fiber products. Figure 3.3 shows the fibers appearance and character.

It should be noted that the PAN-based and pitch-based fibers are made by different methods: through the use of Polyacrylonitrile (PAN) and from pitch. As a result, their properties are different. More specifically, PAN-based precursor carbon fibre has higher strength than pitch-based carbon fibre which has higher stiffness, in other words, more brittle.

Table 3.2 Carbon fibers used for grout thermal enhancement

No.	Product code	Diameter (μm)	Avg. Length (mm)	Aspect Ratio	Fiber Density (g/cm^3)	Carbon ASTM D5291 %	Type
1	AGM94MF0150	7.2	0.10	14	1.81	95.0	PAN
2	AGM94CF0125	7.2	3.00	417	1.81	95.0	PAN
3	AGM94CF0250	7.2	6.00	833	1.81	95.0	PAN
4	AGM95CF0250	13.8	6.00	435	1.54	95.0	PITCH
5	AGM99MF0150	7.4	0.15	20	1.75	99.5	PAN

Product code	**Carbon fibers tested**
AGM94-0.1mm fiber	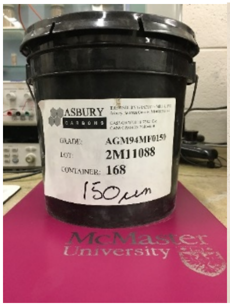 
AGM94-3mm fiber	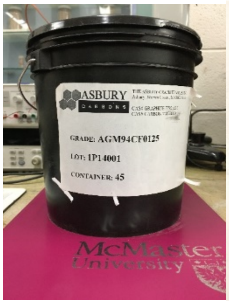 
AGM94-6mm fiber	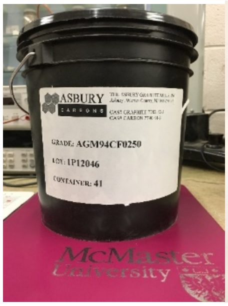 
AGM95-6mm fiber	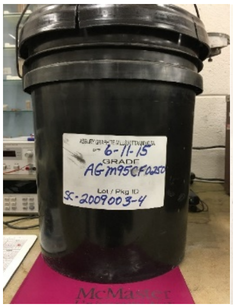 

AGM99-0.15mm fiber	

Figure 3.3 Carbon fibers tested in this research

3.3 Grout thermal conductivity tests

3.3.1 Theory and method

The thermal conductivity test was carried out using the thermal needle probe apparatus described in the ASTM D5334-14 “Standard Test Method for Determination of Thermal Conductivity of Soil and Soft Rock by Thermal Needle Probe Procedure”.

Thermal conductivity was determined by a variation of the line source test method using a needle probe having a large length to diameter ratio to simulate conditions for an infinitely long, infinitely thin heating source. The probe, consisting of a heating element and a temperature measuring element, was inserted into the specimen. Known current and voltage were applied to the probe and the temperature rise with time was recorded over time. The temperature decay with time after the cessation of heating can also be included in the analysis to minimize effects of temperature drift during measurement. Thermal conductivity was obtained from the analysis of the temperature time series data during the heating cycle and cooling cycle if applicable.

If a constant amount of heat is applied to a zero-mass heater over a period of time, the temperature response is:

$$\Delta T = -\frac{Q}{4\pi\lambda} \cdot Ei\left(-\frac{r^2}{4Dt}\right), \qquad 0 \le t \le t_1, \qquad Equation\ \ (3.1)$$

where:

t = time from the beginning of heating (s),
ΔT = change in temperature from time zero (K),
Q = heat input per unit length of heater (W/m),
r = distance from the heated needle (m),
D = thermal diffusivity (m^2/s),
λ = thermal conductivity (W/(m·K)),
Ei = exponential integral, and
t_1 = heating time.

The most direct and precise method to calculate thermal conductivity was to use Equation (3.1) directly with the time series data collected. Unfortunately, λ and D cannot be solved explicitly so that a non-linear least-squares inversion technique must be used. A simplified analysis, which gave adequate results, approximated the exponential integral in Equation (3.1) by the most significant term of its series expansion:

$$\Delta T \cong \frac{Q}{4\pi\lambda} \cdot \ln(t)\,, \qquad 0 \leq t \leq t_1, \qquad Equation\ \ (3.2)$$

For thermal needle probes with diameter of 2.54 mm or less (2mm in this research), the first 10 to 30 seconds of data were excluded from the analysis. The duration of the non-linear portion of initial data was identified and excluded. These data were most strongly affected by terms ignored in Equation (3.2), which resulted in decreased accuracy if they were included in the subsequent analysis. The total time duration of the data included in the analysis, and duration of initial values excluded from the analysis, were fixed for any thermal needle probe configuration. They were used during calibration and all subsequent thermal conductivity measurements with that probe type to avoid biasing results due to subjective selection of the time range for analysis. The remaining data, the quasi steady state portion, was used to determine the slope, S of a straight line representing temperature versus ln(t). The early and late portions of the test (representing transient conditions and boundary effects, respectively) were not used for the curve fitting, shown in Figure 3.4.

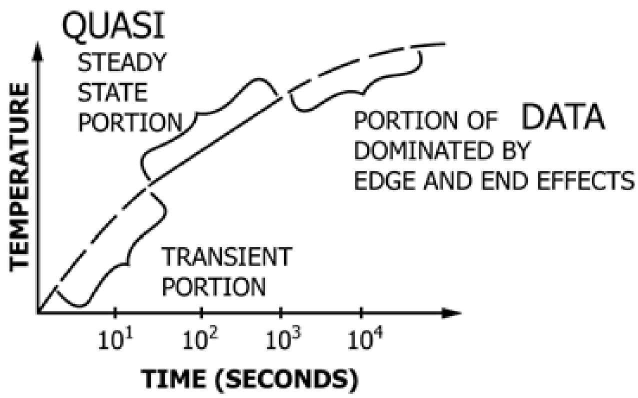

Figure 3.4 Typical record of data

The thermal conductivity, λ, was computed by using:

$$\lambda = \frac{CQ}{4\pi S}, \qquad Equation\ \ (3.3)$$

where S is the slope obtained from quasi steady state portion. It should be noted that C is the calibration coefficient determined as $C = \frac{\lambda_{material}}{\lambda_{measured}}$.

To minimize the probe temperature drifting impact and differentiation derived from randomly distributed fibers in the grout, three measurements were conducted in each specimen and two specimens were produced for each type of grout.

3.3.2 Test setup

The testing system is illustrated in Figure 3.4. The apparatus used in this experiment include: OMEGA T-type probe needle, SOILTEST water bath, HP DC power supply, Agilent data acquisition and software, power-operated paddle mixer, and probe needle stand, as shown in Figure 3.5.

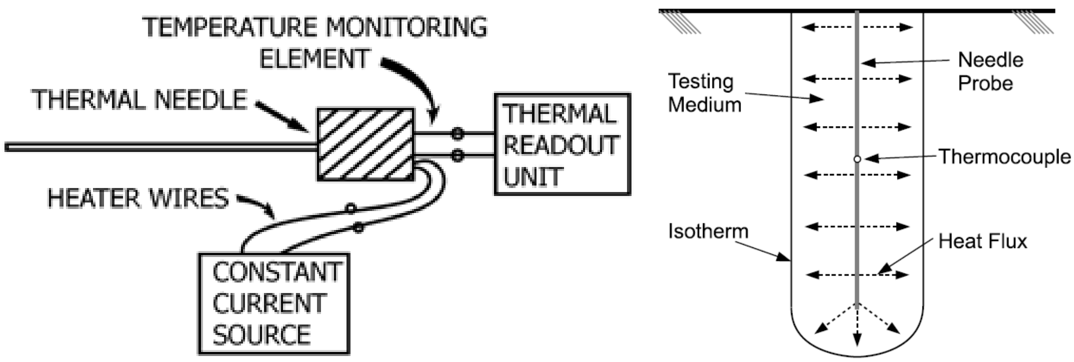

Figure 3.4 Grout thermal conductivity testing system

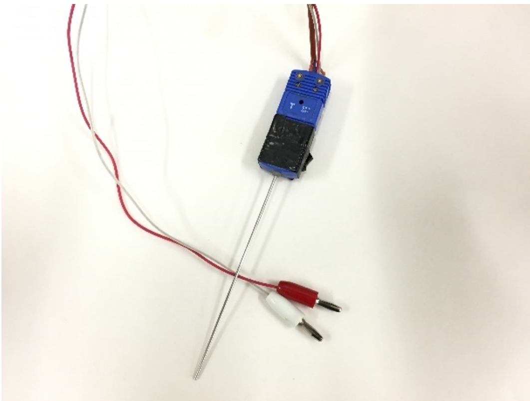

(a). OMEGA T-type probe needle

(b). SOILTEST water bath

(c). HP DC power supply

(d). Agilent data acquisition

(e). Power-operated paddle mixer (f). Probe needle stand

Figure 3.5 Experimental apparatus of grout thermal conductivity test

The 4 different volumetric percentages of carbon fibers added in the baseline grout were 0.5%, 0.75%, 1% and 1.25%, respectively. Detailed volumetric percentages for different grout components are given in Table 3.3. The non-fiber baseline grout consisted of 11.5% bentonite powder, 11.5% sand and 77% de-aired water on volumetric percentage. This combination is referred from the recommended grout treatment by Baroid. For composite grouts with carbon fibers added, a certain amount of industrial sand is replaced by carbon fibers of the same volume. In other words, the volume of bentonite powder and de-aired water in the composite grout was kept constant for all grouts.

Table 3.3 Components volumetric percentages (%) of testing composite grout

Composite Grout	Bentonite Powder	De-aired Water	Industrial Sand	Carbon Fibers
Baseline	11.5	77	11.5	0
1	11.5	77	11	0.5
2	11.5	77	10.75	0.75
3	11.5	77	10.5	1
4	11.5	77	10.25	1.25

Samples of bentonite-sand-carbon fiber composite grout used to measure the thermal conductivity were fabricated by the following steps:

(a) Dry mix industrial sand and bentonite powder with carbon fibers thoroughly based on designed volumetric fractions;

(b) Add required amount of de-aired water into the bentonite-sand-carbon fiber mixture and mix using the power-operated paddle mixer for at least 3 minutes;

(c) Pour the mixed composite grout continuously into cylindrical PVC containers (two containers for each grout) and minimize the amount of trapped air in the grout;

(d) Vacuum the composite grout for at least two hours to remove trapped air during mixing and pouring procedures, under a vacuum pressure of no less than -70 kPa;

(e) Place the samples in a temperature-controlled (set as 30 °C) water bath for at least 24 hours;

(f) Measure the thermal conductivity of composite grout samples in the water bath.

Figure 3.6 gives an illustration of the grout sample producing procedures and measurement in geotechnical laboratory at McMaster.

(a). Mix designed amount of ingredients

(b). Dry mix thoroughly

(c). Use paddle mixer with required de-aired water

(d). Pour grout into PVC containers

(e). Vacuum grout samples (f). Seal and place samples in waterbath

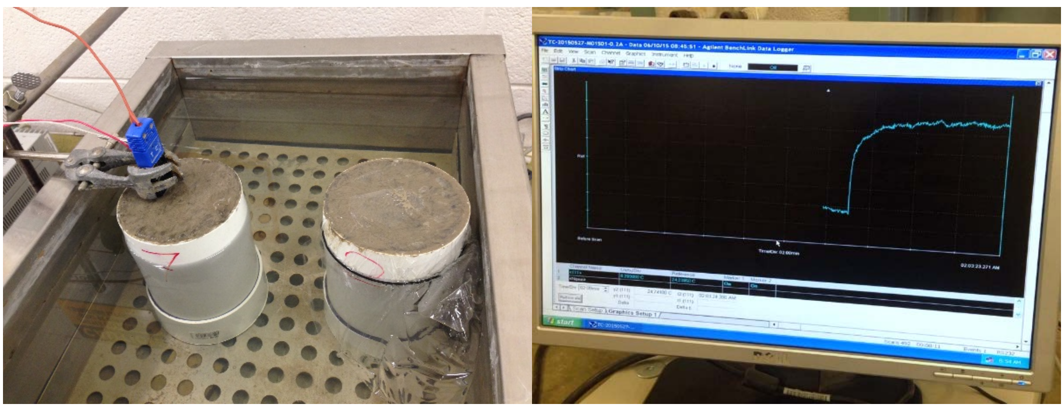

(g). Measure grout thermal conductivity (h). Temperature curve shown in software

Figure 3.6 Experiment procedures of grout thermal conductivity test

Three measurements of temperature were conducted on each cylindrical sample from uniformly spaced locations, providing a total six recorded thermal conductivity values per composite grout mixture. Figure 3.7 presents the locations of the measurement points in a representative grout-filled cylindrical PVC container.

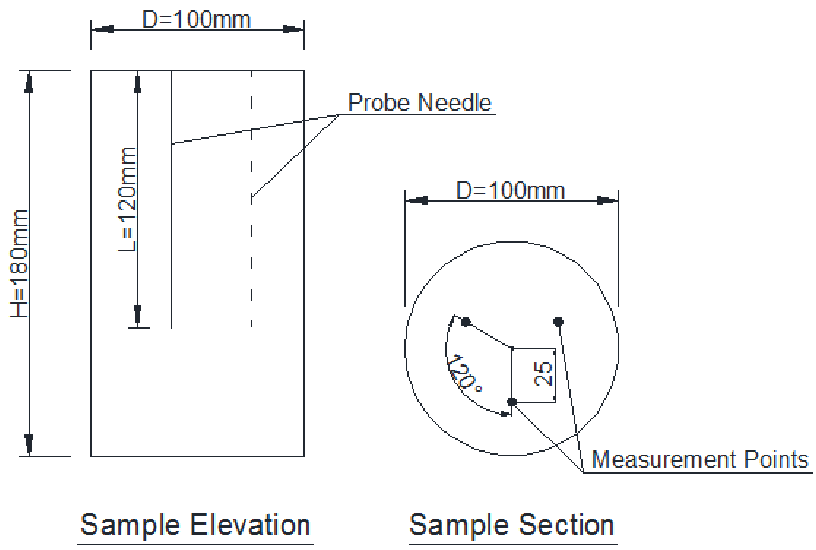

Figure 3.7 Illustration of sample measurement points in a PVC container

3.4 Grout specific heat capacity tests

3.4.1 Theory and methodology

This test is based on ASTM E1269-11 “Standard test method for determining specific heat capacity by differential scanning calorimetry”. The testing method consists of heating the test material at a controlled heating rate in a controlled atmosphere through the region of interest. The difference in heat flow into the test material and a reference material or blank due to energy changes in the material is continually monitored and recorded. Figure 3.8 shows typical heat flow curves of reference material, sapphire standard, and tested material.

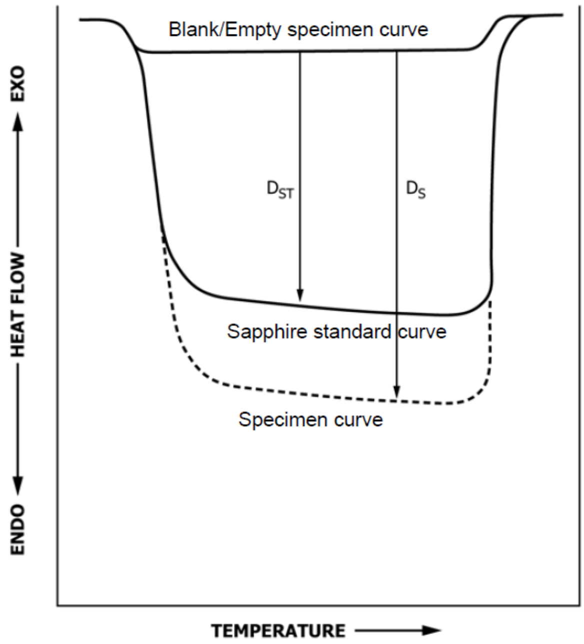

Figure 3.8 Typical heat flow curves for specific heat capacity calculation

The specific heat capacity calculation steps are as follows:

(a). Measure D_{st}, between the empty specimen and sapphire standard, and D_s, between the empty specimen and test specimen, at temperature T;

(b). Calculate calorimetric sensitivity E using below equation:

$$E = [b/(60 \cdot D_{st})][W_{st} \cdot C_p(st) + \Delta W \cdot C_p(c)], \qquad Equation\ \ (3.4)$$

where:

b	=	heating rate, °C/min,
Cp(st)	=	specific heat capacity of the sapphire standard, *J/(g*K)*,
Cp(c)	=	specific heat capacity of the specimen holder, *J/(g*K)*,
E	=	calorimetric sensitivity of the DSC apparatus,
Dst	=	vertical displacement between the specimen holder and the sapphire DSC thermal curves at a given temperature, mW,
Wst	=	mass of sapphire, mg, and
Δ*W*	=	difference in mass between the empty specimen holder and the standard specimen holder, mg, in cases where two sealed specimen holders have to be used or in cases where the empty specimen holder is not also used as the standard specimen holder.

(c). Calculate the specific heat capacity of the test specimen as follows:

$$C_p(s) = \left[\frac{60 \cdot E \cdot D_s}{W_s \cdot b}\right] - \left[\Delta W \cdot \frac{C_p(c)}{W_s}\right], \quad Equation\ \ (3.5)$$

where:

Cp(s)	=	specific heat capacity of the specimen, *J/(g*K)*,
Ds	=	vertical displacement between the specimen holder and the specimen DSC thermal curves at a given temperature, mW,

3.4.2 Test setup

The apparatus used in this test included a TA Instruments Q20 Differential Scanning Calorimeter (DSC), RCS40 refrigerated cooling system, Tzero hermetic aluminum pans and lids, Tzero DSC sample encapsulation press, and high-accuracy digital mass balance, as shown in Figure 3.9.

(a). TA Instruments Q20 DSC with an RCS40

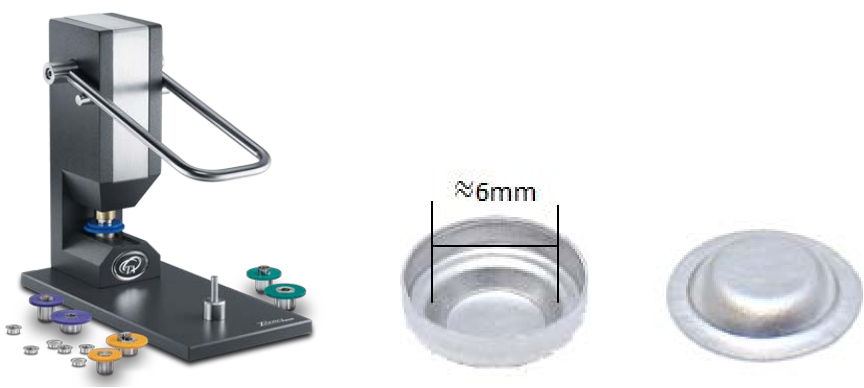

(b). TA Instruments Sample Encapsulation Press and a pair of pan and lid

Figure 3.9 Experimental apparatus of grout specific heat test

Specific heat capacity is a quantitative measurement of energy made as a function of temperature. Thus, the instrument used in its measurement must be calibrated in both temperature and heat flow modes. The Q20 DSC used in this research was calibrated periodically by qualified individuals.

The steps of grout specific heat capacity test are listed as below:

(a) Weigh the mass of a pair of empty Tzero hermetic aluminum pan and lid on the high-accuracy digital mass balance;

(b) Fill in a suitable amount of testing material (bentonite powder, industrial sand, carbon fibers, and composite grout produced in previous thermal conductivity test) to the Tzero hermetic aluminum pan;

(c) Seal the pan with the lid by using Tzero DSC sample encapsulation press.

(d) Weigh the mass of the grout-filled Tzero hermetic aluminum container and another empty reference Tzero hermetic aluminum container;

(e) Place both Tzero hermetic aluminum containers on the corresponding platform in the cooling/heating cell in the DSC.

(f) Input appropriate testing parameters, such as heating/cooling type, sample mass, heating rate, and operating temperature range, in the software and run the test to record the heating flow in respect of temperatures.

Figure 3.10 shows the brief steps of grout specific heat test in chemistry lab at McMaster. Table 3.4 provides detailed mass of each tested samples and containers.

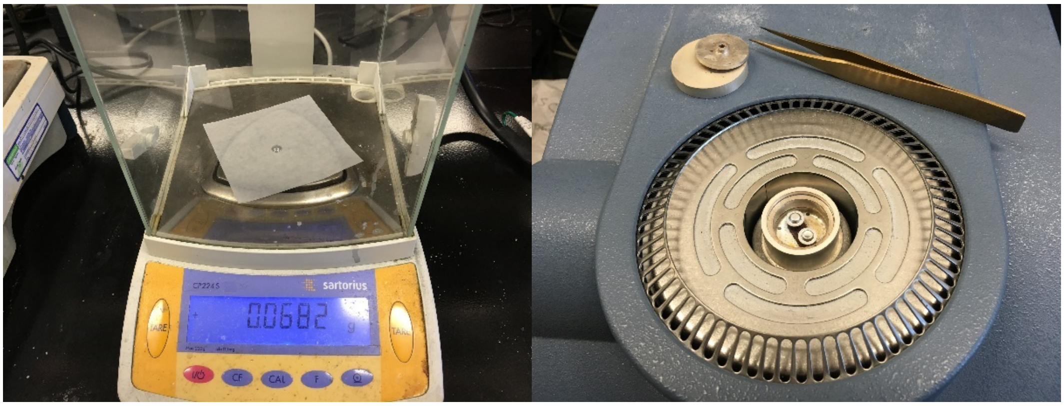

(a). Weigh sample and Tzero container mass (b). Place in DSC heating/cooling cell

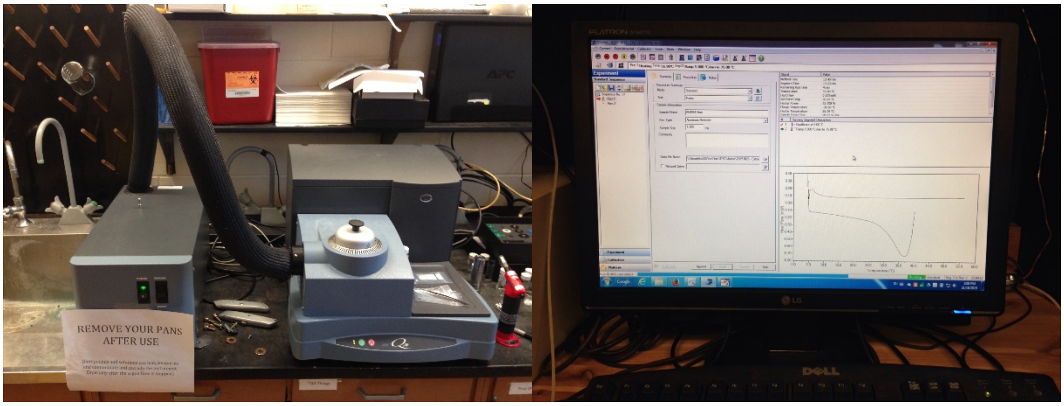

(c). Input required parameters and run test (d). Heat flow curve shown in software

Figure 3.10 Brief laboratory steps of grout specific heat capacity test

The specific heat capacity of the tested grout was determined by measuring the heat flow at a given grout temperature and under a given heating rate of 5 °C per minute. The temperature ranged from 10 to 50 °C. Two samples were tested for each type of grout. A test on the reference material, standard sapphire, was required to calibrate the DSC system before grout sample data analysis and specific heat capacity calculation per ASTM E1269-11.

Table 3.4 Mass of tested samples and Tzero aluminum hermetic containers

Item		*Standard Sapphire*	*Bentonite Powder*	*Industrial Sand*	*AGM94-0.1mm*	*AGM99-0.15mm*
Pan + Lid		46.1	46.3	45.4	46.1	46
Sample		22.1	16.3	64.2	4.2	9.7
V=0%		*Baseline*				
1	Pan+Lid	46.8				
	Sample	30.3				
2	Pan+Lid	46.1				
	Sample	39.8				
V=0.5%		*AGM94-0.1mm*	*AGM94-3mm*	*AGM94-6mm*	*AGM95-6mm*	*AGM99-0.15mm*
1	Pan+Lid	46.1	45.8	45.1	45.8	46.1
	Sample	19.4	12.4	20.8	24.3	17.2
2	Pan+Lid	46.1	45.2	46.1	46.4	46.1
	Sample	23.5	25.6	34.3	27.2	30
V=0.75%		*AGM94-0.1mm*	*AGM94-3mm*	*AGM94-6mm*	*AGM95-6mm*	*AGM99-0.15mm*
1	Pan+Lid	45.6	46	45.5	45.5	46.3
	Sample	26.8	11	19.3	20.4	35.7
2	Pan+Lid	46.5	45.5	45.4	45.9	45.3
	Sample	19	19.5	25	26.7	25
V=1%		*AGM94-0.1mm*	*AGM94-3mm*	*AGM94-6mm*	*AGM95-6mm*	*AGM99-0.15mm*
1	Pan+Lid	45	46.1	46.1	46.1	45.8
	Sample	15.8	20.2	22.5	15.6	15.6
2	Pan+Lid	46.4	45.7	45.9	46.1	45.8
	Sample	21.3	23.6	15.7	19.3	29.6
V=1.25%		*AGM94-0.1mm*	*AGM94-3mm*	*AGM94-6mm*	*AGM95-6mm*	*AGM99-0.15mm*
1	Pan+Lid	45.6	45.2	45.7	46.2	45.7
	Sample	31.5	8.6	22.7	13.9	29.8
2	Pan+Lid	46.2	46.1	46.3	46.1	46.1
	Sample	30.8	22.4	18.4	12.4	10.9

Note:

1. Unit: mg;

2. The reference empty Tzero aluminum hermetic container is 46.1 mg.

CHAPTER 4 EXPERIMENT RESULTS AND ANALYSIS

This chapter summarizes the laboratory test results of thermal conductivity and specific heat capacity of various bentonite-based grouts with different carbon fiber enhancements. The experimental data from past McMaster University research (Tiedje and Guo, 2014) relevant to this study were referred and used when interpreting and analyzing the laboratory test results.

4.1 Grout thermal conductivity test

In GHPS, the thermal conductivity of grout is generally considered as a key parameter to evaluate the thermal efficiency of the whole system. It can also be used to approximately estimate the required ground loop/borehole pipe length. The thermal conductivity is important for GHPS design when selecting the grouting material. Usually the higher the grout thermal conductivity, the better the thermal performance of the system.

In this study, the high thermal conductivity carbon fiber is mixed into bentonite-based grout to find its effect on enhancing the thermal conductivity of composite grout. The influence of fiber volumetric concentration, fiber length, fiber aspect ratio, and fiber carbon content on thermal conductivity are all investigated.

4.1.1 Calibration of thermal needle probe apparatus and baseline grout

According to ASTM D5335-14, the thermal needle probe apparatus should be calibrated before use. The calibration was carried out by measuring both the conductivity of a reference material, standard glycerol in this research, and the grouts with Baroid recommended treatment.

By using the thermal needle probe apparatus, the measured thermal conductivity of glycerol for different heat input (Q=V·A) conditions are shown in Table 4.1. Based on the test results, the thermal needle probe calibration coefficient was determined to be 0.915.

Table 4.1 Calibration by measuring standard glycerol thermal conductivity

Test #	Heat input condition		TC	Mean	Reference	**Calibration**
	Voltage (V)	Current (A)	(W/m·K)	value	value	**coefficient**
1	0.66	0.10	0.323	0.313	0.286	**0.915**
2	0.95	0.15	0.309			
3	1.27	0.20	0.307			

Three grouts were developed based on the treatment table provided by Baroid as shown in Figure 3.1, and the research conducted by Tiedje and Guo (2014). They used a baseline grout which had a 1:1 volumetric ratio of bentonite powder to industrial sand, the same materials introduced in Chapter 3.2, to test the thermal conductivity enhancement effect of several additives such as graphite flake and carbon fibers. To compare the test results with what they found, the 1:1 volumetric ratio of bentonite to sand of the baseline grout is also applied in this study.

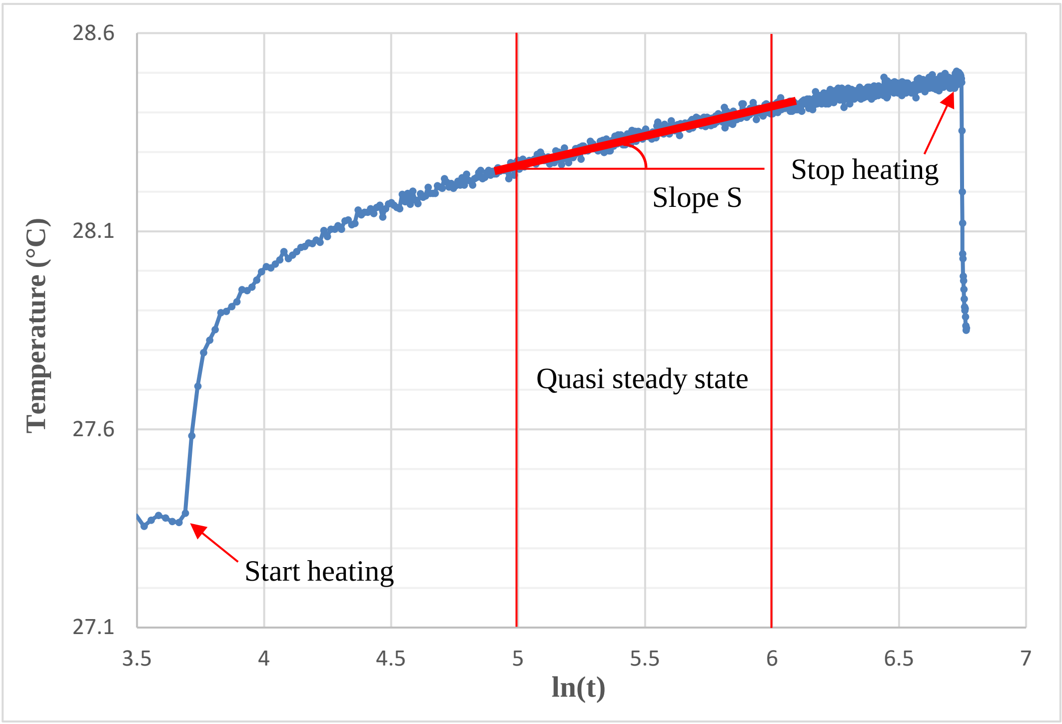

Figure 4.1 Typical testing result on $T - \ln(t)$ plane

Figure 4.1 represents a typical data curve on the T vs ln(t) plot. The quasi steady state portion of the curve which usually appears in the middle part was selected to obtain the slope, S, for calculating sample grout thermal conductivity λ via Equation 3.3 of Chapter 3. In this equation, the heat input Q is available from the test. The calibration coefficient C has been determined to be C=0.915.

Considering the thermal needle probe calibration coefficient C, Table 4.2 shows the measured mean thermal conductivities of non-fiber added grouts with volumetric ratio of bentonite to industrial sand of 1:0, 1:1 and 1:2, and the reference values from Baroid. The measured mean values were very close to those from Baroid, which shows that the apparatus and the testing method used in this study are reliable.

Table 4.2 Measurements of composite grout thermal conductivity

Grout Type	Sample No.	Measurement Results (W/m·K)			**Mean value**	Baroid reference
		Point 1	Point 2	Point 3		
1 : 0	1	0.695	0.673	0.693	**0.68**	0.69
	2	0.558	0.671	0.787		
1 : 1	1	0.867	0.999	0.977	**0.919**	0.94
	2	0.870	0.979	0.820		
1 : 2	1	1.416	1.178	0.988	**1.14**	1.19
	2	0.913	1.417	0.929		

Note:

1. The "Grout Type" in this table represents the volumetric ratio of bentonite powder to industrial sand;

2. The amount of water used is the same for all three grouts based on Baroid recommended grout treatment;

3. The value of Baroid reference for 1:1 ratio grout, 0.94, is derived from interpolating between the values of 1:0 and 1:2 ratio grouts;

4. The measurements were conducted under room temperature in Geo-Laboratory.

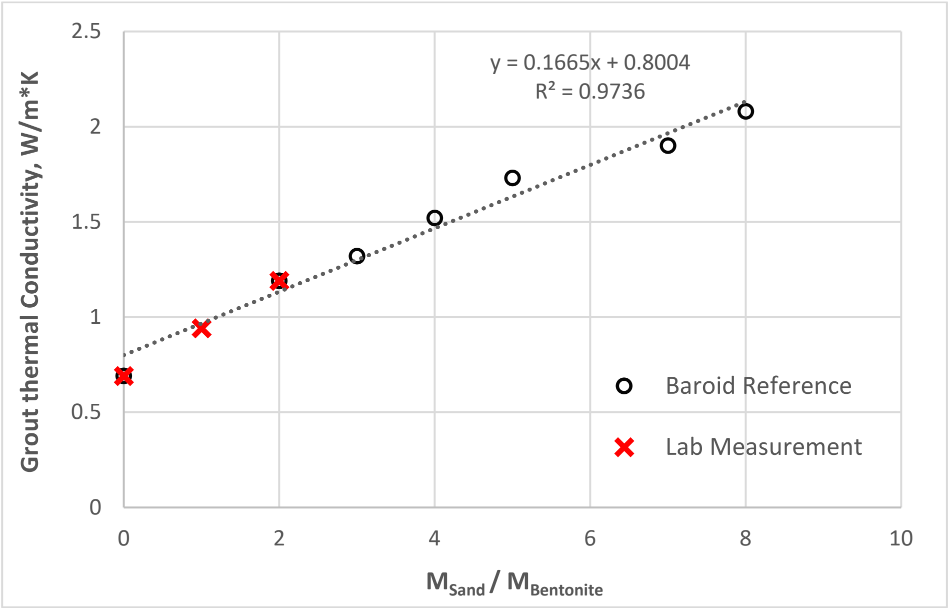

Figure 4.2 Grout thermal conductivities comparison

Regarding Figure 4.2, the grout thermal conductivity of the grout mixtures obtained from laboratory tests are consistent with those provided by Baroid. The measured mean value of the baseline grout with 1:1 bentonite to industrial sand ratio is almost on the dashed trend line corresponding to supplier's reference thermal conductivities of the grout. As a result, it was assumed that it would be reasonable to use 0.919 W/m·K as the baseline grout thermal conductivity for further comparisons.

4.1.2 Effect of carbon fiber additives

Figure 4.3 (a)-(d) summarize the enhancement to thermal conductivity by different types of carbon fibers at various volumetric fiber contents. For each case, six measurements are presented with the mean values shown as short red bars and connected by a red line. The intervals of 95% confidence are also provided in the figures.

For grouts enhanced by 3mm-long and 6mm-long fibres, the measured thermal conductivity varied over a large range, while the data corresponding to the short fibres, 100μm and 150μm, varied over a much smaller range. The main reason for this scatter is attributed to the fibers' orientations relative to the direction of global heat flow, and fibers' aspect ratio. These factors affect the grout thermal conductivity substantially, per the findings by Tiedje and Guo (2014) as well as Demain and Issi (1993).

When the orientation of fibers was parallel to the global thermal gradient, the composite thermal conductivity in the direction of the global thermal gradient increased with the aspect ratio; while for fibers with perpendicular orientation to the global thermal gradient, the composite thermal conductivity tended to decrease with increasing fiber aspect ratio.

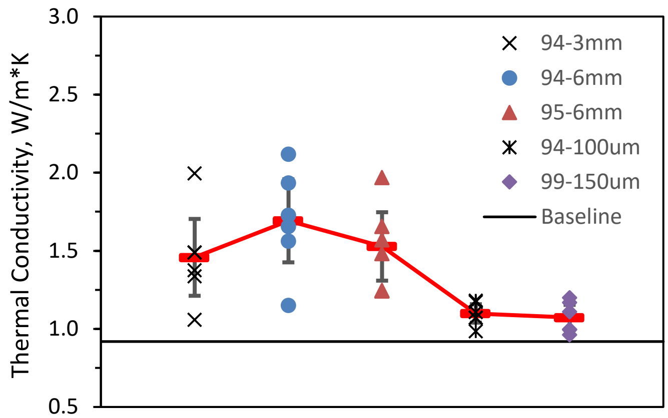

(a) Carbon Fiber Volume 0.5%

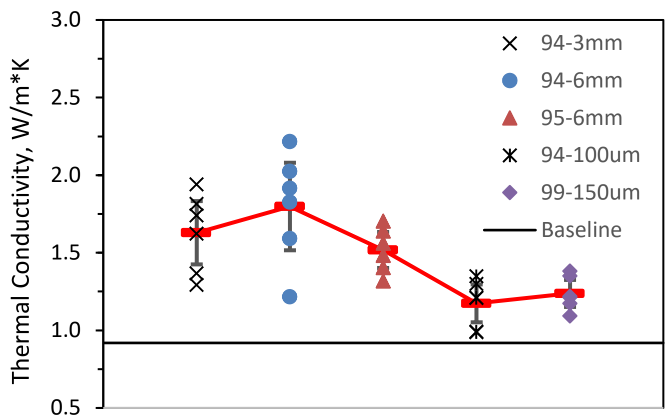

(b) Carbon Fiber Volume 0.75%

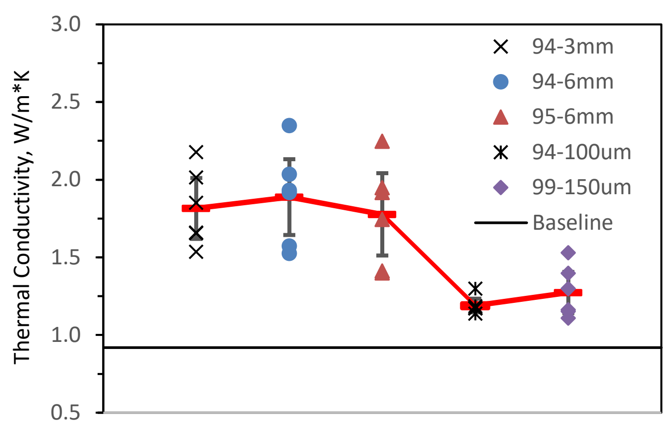

(c) Carbon Fiber Volume 1%

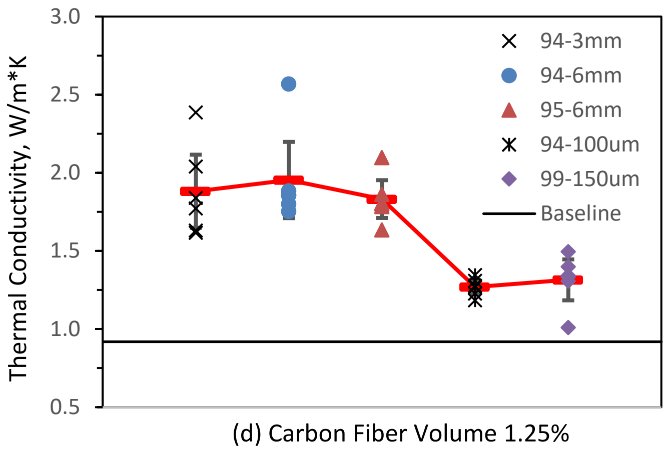

Figure 4.3 Influence of carbon fiber volumetric fraction on grout thermal conductivity for different fiber types

Table 4.3 Mean values of grout thermal conductivity, W/(m*K)

Fiber V%	*94-3mm*	***94-6mm***	*95-6mm*	*94-100µm*	*99-150µm*
0	0.919 (Baseline grout)				
0.5%	1.458	1.692	1.528	1.099	1.073
0.75%	1.629	1.798	1.518	1.174	1.238
1%	1.815	1.888	1.777	1.19	1.274
1.25%	1.882	**1.954**	1.832	1.269	1.315

Figure 4.4 shows the influence of volumetric carbon fiber content on the thermal conductivity of the composite bentonite-based grout. Compared with the thermal conductivity of the baseline grout (without carbon fiber enhancement), the addition of

carbon fiber is seen to increase the thermal conductivity of composite grout in all cases. According to the lab results, for all types of carbon fibers, higher composite grout thermal conductivity was obtained with higher carbon fiber volumetric content.

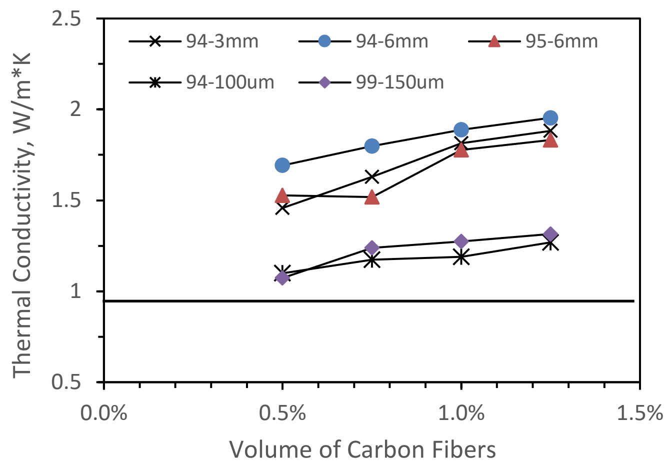

Figure 4.4 Mean values of fiber-added grout thermal conductivity at different fiber volumetric fractions

In particular, AGM94-6mm fiber had the best enhancement effect. By adding only 0.5% by volume AGM94-6mm fiber, the thermal conductivity of the composite grout was increased by more than 80% from barely over 0.9 W/m·K to approaching 1.7 W/m·K. When the carbon fiber percentage increased to 1.25%, the composite grout thermal conductivity was as high as 1.95W/m·K, more than doubled. On the other hand, AGM94-3mm fiber had a greater rate of grout thermal conductivity variation with increasing the fiber content. For the same volumetric fiber content, longer fibers have better enhancement effect than short fibers.

For comparison purposes, the laboratory test results for the composite grouts containing AGM94-3mm and AGM94-100μm fibers obtained in the past study by Tiedje and Guo (2013) are also presented in Figure 4.5. The measured mean values of grout thermal conductivity in both studies are consistent in the range of fiber content between 0.5% and 0.7%, and a similar trend of thermal conductivity with increasing fiber content is clearly observed in the figure.

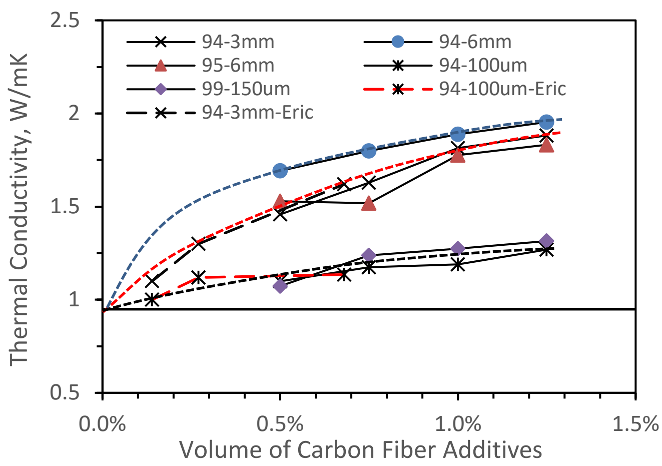

Figure 4.5 Mean values of carbon fiber-added grout thermal conductivity with past research laboratory results from Tiedje and Guo (2013)

The enhancement to composite grout thermal conductivity by fibers of different lengths and aspect ratios are presented in Figure 4.6. It is observed that higher thermal conductivity is obtained by adding longer carbon fibers. For the family of AGM94 fibers, it is as much as 15% more efficient to use 6mm fiber than 3mm fiber in enhancing composite grout thermal conductivity, at the same volumetric fraction.

While 3mm fiber is significantly more efficient than 100μm fiber by up to 50%.

The aspect ratio of carbon fiber is also an important factor that affects the grout thermal performance. As shown in Figure 4.6, for a given fiber volumetric fraction, the use of larger aspect ratio fibers yielded higher thermal conductivities. AGM94-6mm fiber that has the greatest aspect ratio (833) was found to be the most efficient additive to enhance the thermal conductivity of composite grout.

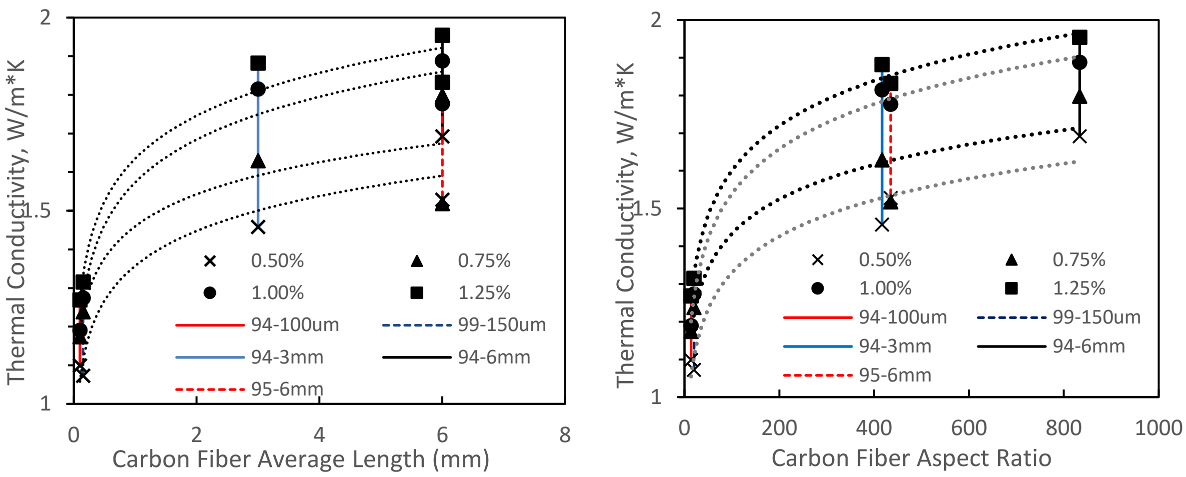

Figure 4.6 Influence of carbon fiber length and aspect ratio on grout thermal conductivity

It should be noted, however, despite no obvious difference between AGM94-3mm fiber and AGM95-6mm fiber on the contribution to grout thermal conductivity enhancement, the AGM95-6mm fiber which had a larger aspect ratio (435) was less effective than the AGM94-3mm fiber, which had a smaller aspect ratio (417). The relatively poor enhancement effect of AGM95-6mm fiber was mainly attributed to its

"Petroleum Pitch (Pitch)" type instead of "Polyacrylanitrile (PAN)" type, the type of all the other fibers. This Pitch type carbon fiber had a much lower tensile strength and Young's modulus. More specifically, per fiber product data from Asbury Carbon, the Pitch type fibers tensile strength and Young's modulus were only 10% and 15% compared with those of PAN type fibers, respectively. It was likely that fiber breakage took place when the fibers were mixed with sand and bentonite powder by using power paddle mixer. Therefore, the equivalent fiber length in composite grouts with AGM95-6mm could possibly have been shorter than the nominal 6mm length, leading to a smaller fiber aspect ratio and hence lower grout thermal conductivity. The breakage of AGM95-6mm fibers was observed in the examination of some post-mixed grout samples.

4.1.3 Non-sand composite grout

According to the literature review, the addition of sand in bentonite grouts can increase grout thermal conductivity to a reasonable level and permeability as well. However, high grout permeability is not expected in most practical GHPS applications. The test results in this research confirmed that the addition of a small fraction of carbon fibers could reduce the fraction of sand used in grout without sacrificing grout thermal conductivity. Based on this, a non-sand bentonite-based grout with carbon fibers was investigated to explore the possibility of manufacturing non-sand composite grouts without sacrificing thermal conductivity.

Three types of non-sand composite grouts were tested using 0.5% and 1.0% carbon fiber content. Compared with the $M_{Sand}/M_{Bentonite}$≈1 grout, Type A grout contained the same volumetric ratio of bentonite powder to de-aired water, 11.5:77=13:87; while Type B grout had the same volumetric ratio of solids to de-aired water, 23:77. The 0.5% fiber volume came from that of bentonite powder in both composite grout A and grout B. The fiber content in Type C grout was increased from 0.5% to 1% where the additional 0.5% volume was also from that of bentonite powder.

The volumetric percentages of different ingredients in non-sand grouts are listed in Table 4.4.

Table 4.4 Non-sand grout materials volumetric fractions (%)

Grout Type	Bentonite powder	De-aired water	Carbon fiber	Sand
A	12.5	87	0.5	0
B	22.5	77	0.5	0
C	12.0	87	1.0	0
$M_{sand}/M_{bentonite}$≈1	11.0	77	0.5	11.5

Table 4.5 Mean thermal conductivity of non-sand grout and baseline (W/m·K)

Grout Type	**AGM94-0.1mm**	**AGM94-3mm**	**AGM94-6mm**
A	0.844	1.035	1.081
B	0.959	1.261	1.373
C	0.896	1.184	1.261
$M_{sand}/M_{bentonite}$≈1	1.099	1.458	1.692

Note:

1. The bentonite to sand volumetric ratio in $M_{sand}/M_{bentonite}$≈1 grout is 11.0:11.5.

Table 4.5 summarizes the laboratory results of the mean thermal conductivity values of non-sand composite grouts. Owing to its low solids content, Type A grout thermal conductivity was lower by 30% when compared to the $M_{Sand}/M_{Bentonite}$≈1 grout thermal conductivity. Although Type B grout had the same solids content as the $M_{Sand}/M_{Bentonite}$≈1 grout does, its thermal conductivity only approaches 90% of baseline grout conductivity. With fiber content being increased to 1%, the thermal conductivity of Type C grout does not show a clear enhancement while the value is even lower than that of Type B grout.

The test results revealed that adding carbon fiber in grout with lower volumetric solid fractions was not as efficient as grout with higher volumetric solid fractions. To reach a high composite grout thermal conductivity with acceptable grout permeability, the use of appropriate amount sand (bentonite to sand as 1:1 volumetric ratio at 11.5% each) in composite grout was found to be reasonable, economical, and applicable. Further investigation is needed to optimize the composite grout to achieve high thermal conductivity and ideal performance regarding permeability, viscosity and pumpability.

4.2 Grout specific heat capacity test

The following analyses focus on the variation of specific heat capacity of bentonite-based grouts blended with carbon fiber content using the differential scanning calorimeter method as described in ASTM E1269-11.

4.2.1 Standard sapphire calibration

Before testing and analyzing composite grout samples, tests on a reference material had to be performed to calibrate the DSC system. A special designed standard sapphire sample that matches the Tzero hermetic container was used for the calibration test.

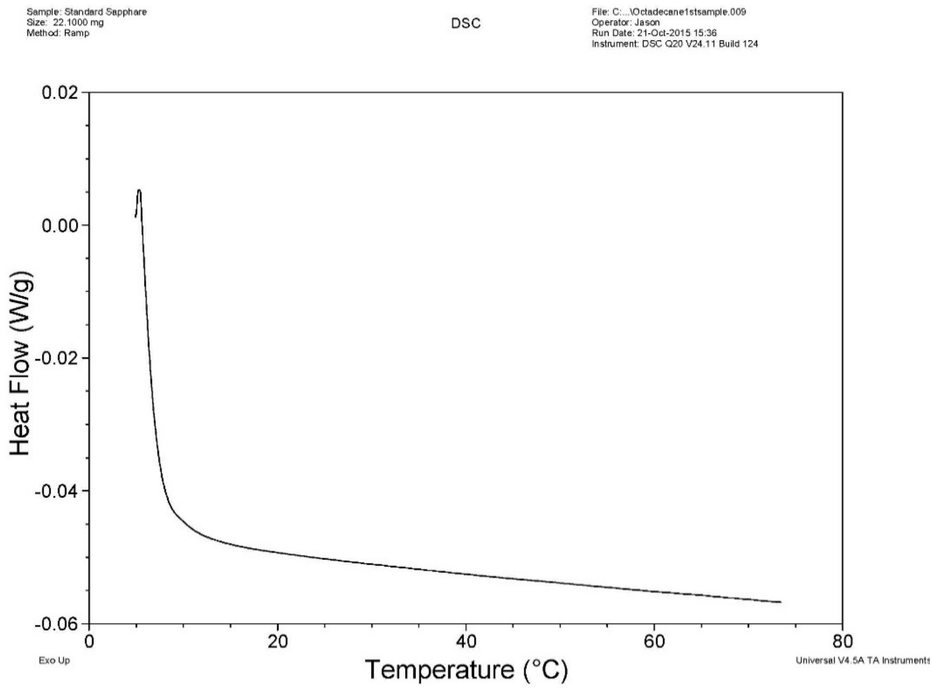

Figure 4.7 Heat flow curve of standard sapphire sample

Figure 4.7 presents a representative heat flow curve of a tested sample using the standard sapphire. The heat flow values at 10°C, 20°C, 30°C, 40°C and 50°C were collected to calculate the sample specific heat capacity at the corresponding temperatures. The specific heat capacities of the standard sapphire and aluminum hermetic containers are provided in ASTM E1269-11. The calibration test was run to obtain the calorimetric sensitivity E of the DSC apparatus. The calorimetric sensitivity, calculated based on Equation 4.1, was subsequently used to calibrate the test and attain the accurate specific heat capacity of tested samples.

$$E=[b/(60 \cdot Dst)][Wst \cdot Cp(st)+\Delta W \cdot Cp(c)] \qquad \text{Equation (4.1)}$$

where:

b is heating rate, 5°C/min in this study;

Dst is the heat flow difference between the DSC curves of empty referred Tzero aluminum hermetic container and the standard sapphire at a given temperature, mW;

Wst is the mass of standard sapphire, mg;

Cp(st) is the specific heat capacity of the standard sapphire, J/(g*K);

ΔW is the mass difference between the empty referred Tzero aluminum hermetic specimen container and the one used to seal standard sapphire, mg;

Cp(c) is the specific heat capacity of Tzero aluminum hermetic container, J/(g*K).

Table 4.6 summarizes the calibration test results of the DSC apparatus. The calorimetric sensitivity E was around 1.22 in the temperature range from 10°C to 50°C. This set of sensitivity values were used to calculate the specific heat capacity of tested composite grouts and ingredient materials.

Table 4.6 Summary of DSC calibration test result

Temperature (°C)		**10**	**20**	**30**	**40**	**50**
Dst (mW)	1	1.184	1.213	1.242	1.271	1.300
	2	1.072	1.101	1.130	1.159	1.188
	Average	1.128	1.157	1.186	1.215	1.244
Cp(st) (J/g*K)		0.745	0.765	0.785	0.805	0.825
Cp(c) (J/g*K)		0.885	0.892	0.899	0.906	0.913
Sensitivity, *E*		**1.216**	**1.218**	**1.219**	**1.220**	**1.221**

Note:

1. The specific heat capacity values, Cp(st) and Cp(c), are referred from ASTM E1269-11;

2. Two calibration tests were conducted by using the same standard sapphire sample.

4.2.2 Composite grouts test results

Per ASTM E1269-11, using calorimetric sensitivity E to calculate the specific heat capacity of the test specimen is as follows:

$$Cp(s)=[(60 \cdot E \cdot Ds)/(Ws \cdot b)]-[(\Delta W \cdot Cp(c))/Ws] \qquad \text{Equation (4.2)}$$

where:

Cp(s) is the specific heat capacity of the tested sample, J/(g*K),

Ds is the heat flow difference between the DSC curves of empty referred Tzero aluminum hermetic container and the tested sample at a given temperature, mW;

Ws is the mass of the tested sample, mg;

ΔW is the mass difference between the empty referred Tzero aluminum hermetic container and the one used to seal tested sample, mg;

Other symbols were defined in Equation 4.1.

Table 4.7 summarizes the measured specific heat capacity, *Cp(s)*, of the composite grout enhanced by different carbon fibers and the materials themselves under temperatures ranging from 10°C to 50°C.

Table 4.7 Summary of specific heat capacity test results

Grout Type		Specific heat capacity, *Cp(s)*, J/(g*K)				
		10°C	20°C	30°C	40°C	50°C
V=0%	Baseline	2.852	3.267	3.684	4.101	4.519
V=0.5%	94-100um	1.908	2.224	2.282	2.342	2.425
	94-3mm	2.914	3.645	4.378	5.111	5.846
	94-6mm	2.911	3.484	4.057	4.632	5.207
	95-6mm	2.572	3.235	3.807	4.475	5.021
	99-150um	1.945	2.462	2.604	2.769	3.044
V=0.75%	94-100um	2.995	3.414	3.741	3.954	4.206
	94-3mm	2.712	3.064	3.414	3.909	4.557
	94-6mm	2.645	3.067	3.521	4.105	4.782
	95-6mm	2.868	3.446	3.982	4.504	5.033
	99-150um	2.157	2.421	2.571	2.727	2.904
V=1%	94-100um	2.995	3.520	4.002	4.429	4.902
	94-3mm	2.573	2.963	3.203	3.482	3.781
	94-6mm	2.650	2.967	3.270	3.584	3.924
	95-6mm	2.576	2.955	3.367	3.894	4.476
	99-150um	2.251	2.470	2.614	2.804	3.028
V=1.25%	94-100um	3.664	4.172	4.624	5.090	5.426
	94-3mm	3.325	3.821	4.024	4.262	4.674
	94-6mm	2.855	3.028	3.133	3.276	3.475
	95-6mm	2.857	3.299	3.685	4.020	4.315
	99-150um	3.385	3.765	4.175	4.605	5.194
Bentonite powder		1.482	1.619	1.724	1.863	2.062
Industrial sand		0.741	0.800	0.827	0.850	0.870
AGM94 fibers		0.903	0.928	0.954	0.979	1.004
AGM99 fiber		0.951	0.992	1.032	1.072	1.113

Note:

*1. The specific heat capacity of water is considered as 4.182 J/(g*K) in this temperature range;*

2. AGM94 and AGM95 fibers contain the same carbon concentration at 95%, and AGM99 fiber has a 99.5% carbon content.

Figure 4.8 presents the specific heat capacity, *Cp(s)* of the various mixtures at different testing temperatures. For comparison purposes, Figure 4.8 also includes the specific heat capacity of dry bentonite powder and the baseline grout with $V_s : V_b : V_{water} = 11.5:11.5:77$ or $M_s : M_b : M_{water} = 22.7:22.7:58.5$.

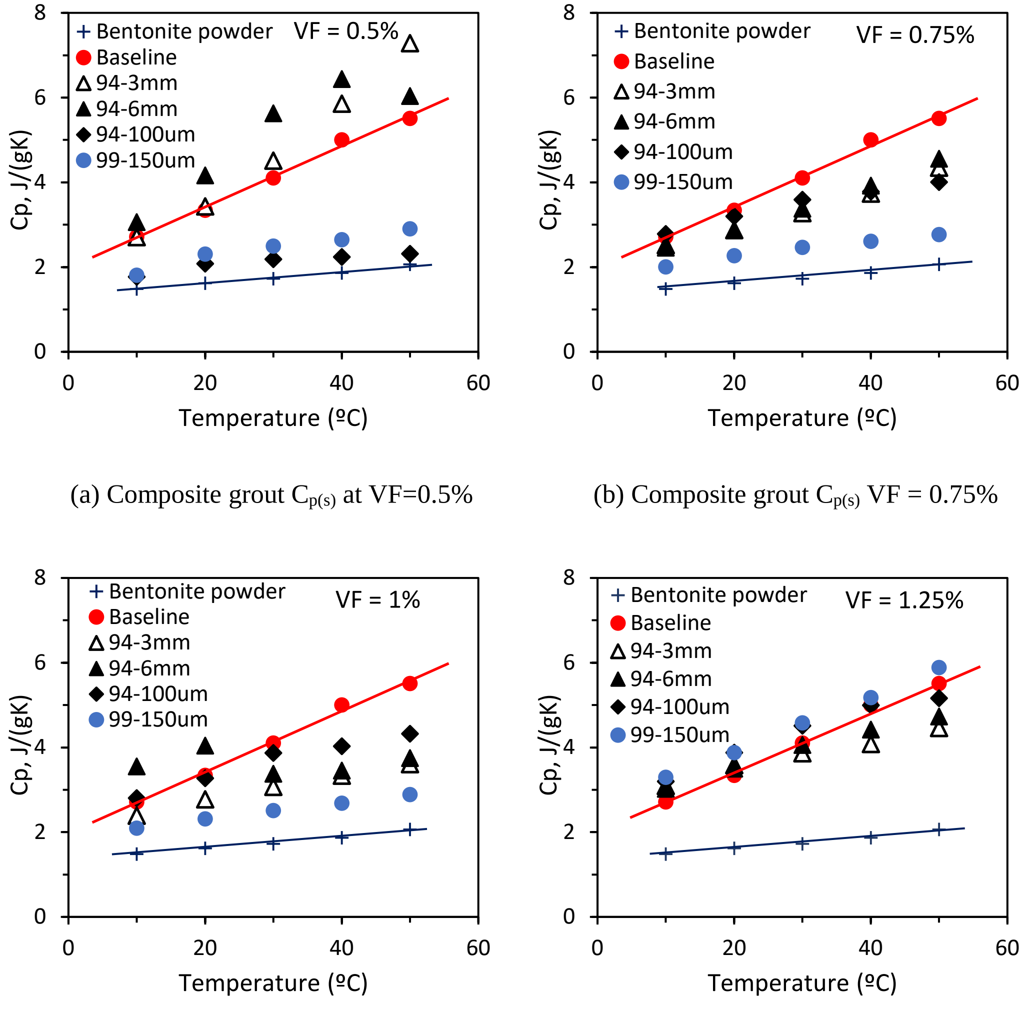

(a) Composite grout $C_{p(s)}$ at VF=0.5%

(b) Composite grout $C_{p(s)}$ VF = 0.75%

(c) Composite grout $C_{p(s)}$ at VF = 1%

(d) Composite grout $C_{p(s)}$ at VF = 1.25%

Figure 4.8 Summary of composite grout specific heat capacity

In general, the specific heat capacity of the grouts with fiber contents of 0.75%, 1% and 1.25% varied between the values of bentonite powder and the baseline grout. The range of variation in specific heat capacity at given volumetric fraction narrowed as the temperature decreased for all cases.

It is interesting to note that adding fiber had marginal effect on the *Cp(s)* of composite grout when compared the baseline case (as shown in Figure 4.9), even though the data are scattered.

The scattered data was attributed to the small amount of grout sample used for DSC heat capacity measurements. The marginal effect of fiber volumetric fraction on the measured *Cp(s)* values can be explained as follows. Based on the test results in Table 4.6, the *Cp(s)* of carbon fibers were approximately 20% higher than those of industrial sand in the testing temperature range, while the specific gravity of sand was 40% greater than that of the fibers. Since volume of industrial sand was reduced ($\leqslant$ 1.25%) to keep a constant solid volume fraction when fiber was added, and the specific heat capacity is a scalar material characteristic related to the mass and temperature only, it was not surprising that most *Cp(s)* of the mixtures were close to those of baseline grout.

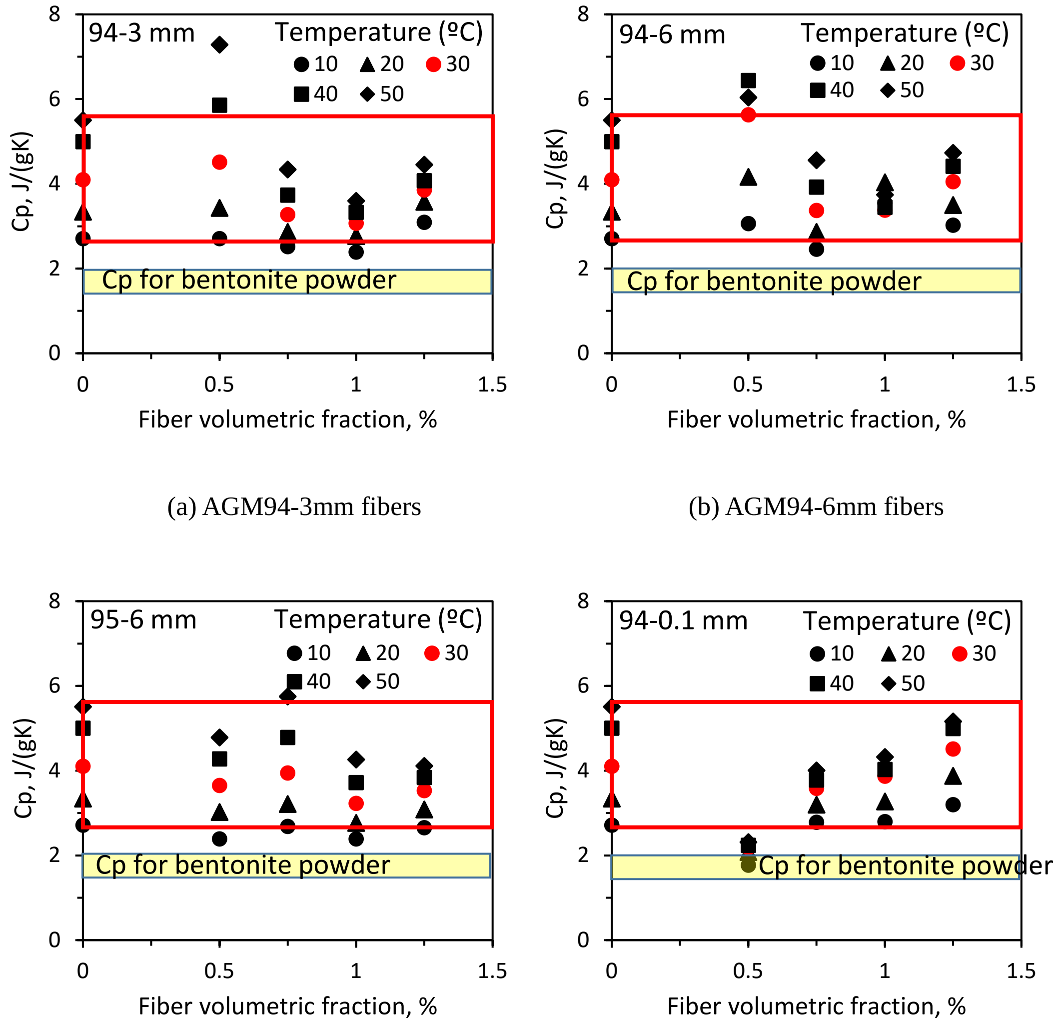

(a) AGM94-3mm fibers

(b) AGM94-6mm fibers

(c) AGM95-6 mm fibers

(d) AGM94-100μm fibers

Figure 4.9 Effect of fiber type and volumetric content on grout specific heat capacity

CHAPTER 5 ON-SITE BENCH SCALE EXPERIMENT AND NUMERICAL SIMULATION

5.1 Industrial on-site bench scale experiment

Based on the huge market potential of the carbon fiber enhanced composite grouting material in the GHPS industry, this study was supported by McClymont & Rak Engineers Inc. ("MCR" hereinafter). A series field bench scale tests, shown in Figure 5.1, were carried out to verify the effect on GHPS by carbon fiber enhanced bentonite grouts developed in previous chapters. The following sections provide the details of this bench scale test and the summary of the field test results from MCR.

Figure 5.1 MCR bench scale experiment

5.1.1 MCR bench scale experiment

The experiment was conducted at MCR, with a near constant ambient temperature of 19 to 20°C during testing period. The bench scale test setup included the following components (See Figures 5.2 to Figure 5.5):

(1). Tank: An insulated cylindrical tank 1.5m high and 1.0m inner diameter was used as the main part of the experiment setup, see Figure 5.2(a). An aluminum core pipe was installed at the centre of the tank, through a concentric round hole at the bottom of the cylindrical tank. The tank was filled with dry sand as soil medium surrounding the pipe.

(2). Aluminum core pipe: The 1.8m long core pipe with a 0.15m internal diameter and 4mm wall thickness was sealed at the bottom end and acted as a borehole in which circulating pipes were placed and grouted.

(3). Fluid circulating pump system: A pump system (Figure 5.2b) was used to circulate the fluid, water for this experiment, in the U-shape geothermal pipe at the flow rate of **24.1** liters per minute.

(4). Heater: To control the energy input to the circulating water, a 750-watt heater (Figure 5.2c) kept running to heat water and supplied a constant volumetric heat flux of **0.521** W/cm^3 during the test.

(5). Geothermal pipe: The single U-shape pipe used in this experiment was high efficiency 1-¼’ GeoPerformX pipe from VERSA PROFILES as shown in Figure 5.3. This pipe, with 34mm inner diameter and 4mm wall thickness, was made from PE3608 polyethylene filled with highly thermally conductive nanoparticles, providing a typical value of **0.7** W/m·K thermal conductivity. The pipe was placed in the aluminum core pipe filled with grouting material, and connected to the fluid circulating pump system (Figure 5.2e).

(a). Insulated Tank (b). Circulating Pump

(c). Fluid Heater

(d). Temperature Sensor Control System

(e). Insulated top cover and geothermal pipes

Figure 5.2 Bench scale test setup

Figure 5.3 VERSAPROFILES GeoPerformX pipe

(6). Composite grouting material: The composite grouting material used in this bench scale test was bentonite-based grout with 1.25% volumetric AGM94-6mm fiber added. The thermal conductivity of this grout is **1.954** W/m·K and the density is 1360.5 kg/m^3.

(7). Soil medium: Dry industrial sand, the same as that used to produce composite grout in previous chapters, was used to fill the tank, acting as soil medium. The temperatures at select locations in the sand were measured continuously during the experiment.

(8). Temperature sensors: The temperature measurement system consisted of 29 temperature sensors, in which 28 were located at select locations in the dry sand, and one installed in the aluminum core pipe at center of the tank. Most sensors in soil were on the horizontal plane at the middle height of the tank (0.75m from tank top/bottom), with the locations being illustrated in Figure 5.4. The locations of the other temperature sensors are presented in the schematic of this bench scale test shown in Figure 5.5.

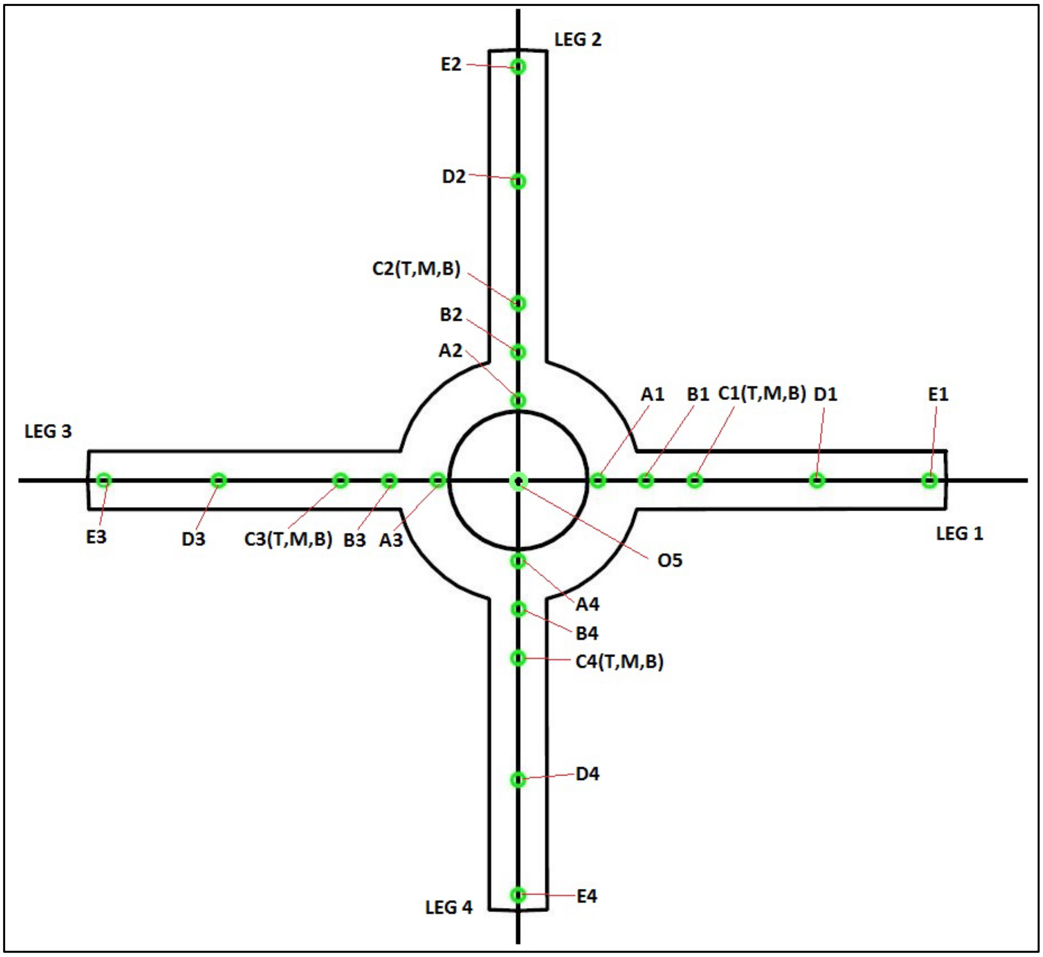

Figure 5.4 Temperature sensors layout (Plane)

In order to measure the temperature distribution and evolution within the sand bed by installing temperature sensors at select locations on the middle horizontal plane, a cross-shaped frame having four legs was designed. Each leg had five sensor points, labelled from A to E as shown in Figure 5.4. Eight additional temperature sensors at locations C1, C2, C3, and C4 were used to measure the temperatures at the top and bottom of the soil.

Details of each sensor point are listed as follows:

1) ***O5***: Located at the center of tank, in the aluminum core pipe, to measure flowing water temperature;

2) ***A1-A4***: Located in dry sand immediately outside of aluminum core pipe, with the radial distance to tank center being 0.08m;

3) ***E1-E4***: Against the inner tank wall, in the dry sand, and the radial distance was 0.5m;

4) ***C1-C4***: Located at the mid-points between *A* and *D*; Placed at three different heights in soil: the top (close to the tank surface), mid-height, and the bottom (close to the tank bottom). The radial distance to tank center was 0.29m.

5) ***B1-B4***: Located at the mid-points of *A* and *C*; The radial distance to tank center was 0.18m;

6) ***D1-D4***: Located at the mid-points of *C* and *E;* The radial distance to tank center was 0.4m.

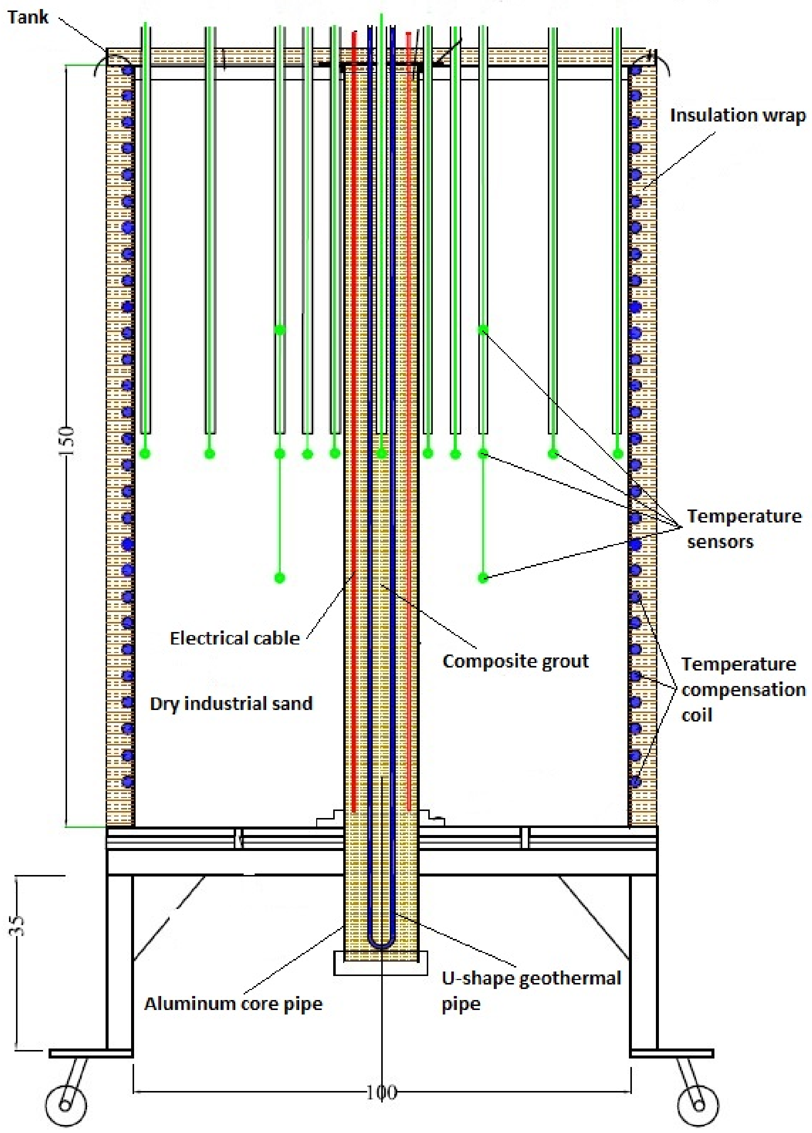

Figure 5.5 Bench scale test schematic

When performing the bench scale test, the temperature data were measured at different locations in the tank. The recorded temperatures were then analyzed to obtain the temperature distribution and to study the heat transfer pattern in the soil medium. The carbon fiber enhanced bentonite-based grout was used to fill the core aluminum pipe (i.e., the borehole). The test continued until the system reached a steady state at which time the measured temperature field did not change for a reasonable long period. Typically, a bench scale test took approximately 4 hours.

5.1.2 Results of MCR bench scale experiment

Three bench scale tests were conducted on January 19th, January 22nd and February 16th 2016. Figure 5.6 presents the steady state soil temperature distribution in the radial direction at the end of each test.

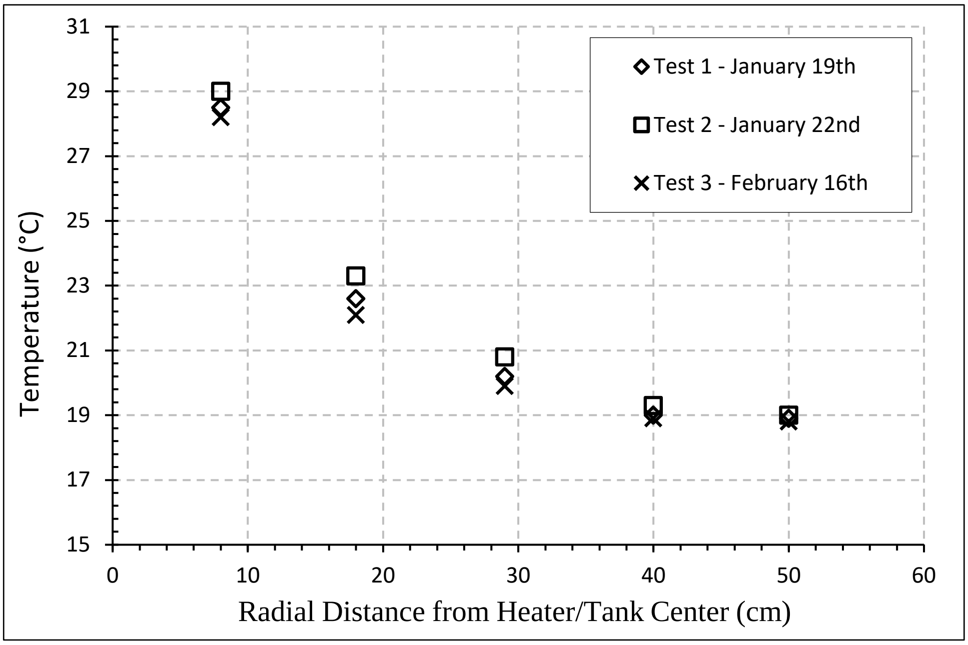

Figure 5.6 Measured temperature distribution of bench scale tests

The temperature values shown are the average of measured temperatures at four points (e.g. ***A1*** to ***A4***, ***B1*** to ***B4***, etc.) which had the same radial distance on each leg. The temperature at center of borehole, Point ***O5***, was 29.9°C, 30.4°C, and 29.4°C for Test 1, Test 2 and Test 3, respectively.

5.2 Numerical simulation of MCR bench scale experiment

Finite element modeling was carried out to simulate the bench scale tests. A general-purposed finite element software ABAQUS was used for numerical simulation.

5.2.1 Heat transfer theory

(1) Governing equations

The term conduction is used to refer to the transport of heat from high temperature to low temperature in a stationary medium, which may be a solid or a fluid, by the motion of molecules or electrons. In an isotropic continuous medium, heat conduction in the *x*-direction is described by Fourier's Law

$$q_x = -\lambda \cdot \left(\frac{\partial T}{\partial x}\right) \qquad \text{Equation (5.1)}$$

where

λ - thermal conductivity, W/m·°C or W/m·K

T - temperature, °C or K

q_x - heat flux in the *x*-direction, W/m^2

$\partial T/\partial x$ – temperature gradient in the *x*-direction, °C/m or K/m

During a heat transfer process, the condition of energy balance requires

Rate of thermal energy accumulation	=	Net rate of thermal energy in by convection	+	Net rate of thermal energy in by conduction

For an isotropic continuous medium, the conservation equation of thermal energy is generally expressed as

$$\frac{\partial(\rho CpT)}{\partial t} = -\nabla \cdot \left(\rho C_p T \boldsymbol{u}\right) - \nabla \cdot \lambda \nabla T \qquad \text{Equation (5.2)}$$

where

ρ – density of material, kg/m^3

C_p - specific heat capacity, J/kg·°C or J/kg·K

t - time, s

u – displacement vector, m

For material with constant specific heat capacity C_p and thermal conductivity λ, Equation 5.2 is rewritten as:

$$\frac{\partial T}{\partial t} + \boldsymbol{u} \cdot \nabla T = K \nabla^2 T \qquad \text{Equation (5.3)}$$

where

K= $\lambda/\rho C_p$, thermal diffusivity, m^2/s.

In reality, the thermal conductivity of a material may be anisotropic, orthotropic, or isotropic. For fiber-enhanced composite grout, the thermal conductivity highly depended on the orientation of fibers. In this study, since carbon fibers were uniformly distributed in the composite grout, the grout thermal conductivity was found to be isotropic from laboratory tests and the measured thermal conductivity value, 1.954 W/m·K, was considered to be representative.

(2) Boundary conditions

Boundary conditions are generally considered to describe the heat flux rate around the outer boundary of the calculation domain. In the finite volume method, each control volume has several control-volume faces around it, and heat flow occurs across these control-volume faces whether the control-volume faces are positioned inside the domain or on the outer boundary of the domain (Hong, 2004).

For the heat transfer occurs between two different subdomains, or the inner boundary, with thermal resistance:

$$q(\equiv -\lambda \frac{\partial T}{\partial x}) = h_{int} \cdot (T_{\Omega 1} - T_{\Omega 2}) \qquad \text{Equation (5.4)}$$

where, h_{int} - interfacial heat transfer coefficient between two subdomains, W/m^{2}·°C

$T_{\Omega 1}$ - surface temperature of the adjacent control volume in subdomain Ω1, °C

$T_{\Omega 2}$ - surface temperature of the adjacent control volume in subdomain Ω2, °C

In this study, the top, bottom, and outer side of the tank, the outer-domain boundaries, are considered to be insulated which means the heat flux rate at these boundaries equals to zero. While the interfaces between different materials, the inner-domain boundaries, are assumed to be ideal contact which means there is no interfacial resistance.

To demonstrate the impact of interfacial resistance, a simplified simulation by assuming an interfacial heat transfer coefficient on the interface between aluminum pipe and sand is provided at the end of this chapter.

5.2.2 Heat transfer analysis in ABAQUS

This bench scale test was treated as an uncoupled heat transfer process. The thermal properties of the different materials used in bench scale test are given in the Table 5.1 (thermal properties are provided by MCR and material specification sheet from vendors). These properties were the necessary input parameters to simulate the heat transfer process numerically.

Table 5.1 Material properties (input parameters)

Properties	**Density (kg/m^3)**	**Thermal Conductivity (W/m·°C or W/m·K)**	**Specific Heat Capacity (J/kg·°C or J/kg·K)**
Fluid (water)[2]	1000	0.631	4180
GeoPerformX[2]	1009	0.7	1958
Composite Grout[3]	1361	1.954	3028
Aluminum Pipe[2]	2700	205	900
Industrial Sand[2]	2623	0.25	800

NOTE:

1. The thermal conductivity and specific heat capacity in this table are under 20°C;

2. The material thermal properties in this table are provided by vendors and MCR;

3. The material properties of composite grout are obtained by laboratory tests.

The bench test was simulated as an axisymmetric thermal conduction problem. Figure 5.7 presents the model of the system with all components, including the tank, soil, the core aluminum pipe, the grout, the GeoPerformX pipe and the circulating water (Heater). The system was discretized by 4-noded bilinear axisymmetric quadrilateral elements, DCAX4, with a temperature degree of freedom at each node. The U-shaped GeoPerformX pipe was represented by a single pipe having the same cross-sectional area to simplify the model building and make it axisymmetric.

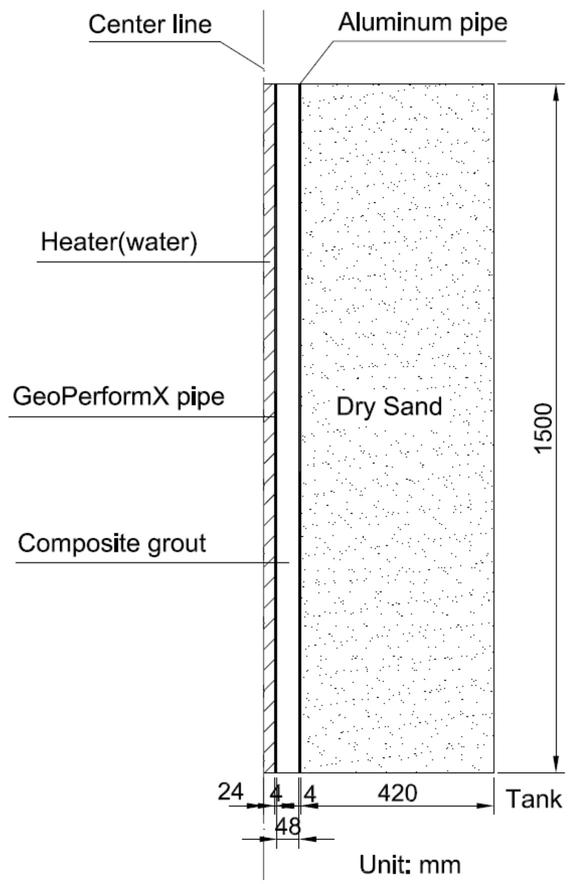

Figure 5.7 Illustration of axisymmetric tank model

The finite element mesh used in the heat transfer analysis for the bench tests was illustrated in Figure 5.8. A total number of 7200 elements with the maximum element size being 2cm were used to discretize the system. An initial temperature of 19°C, the same as the constant ambient temperature at the MCR bench scale test site, was specified for this model. The top, right (i.e. outer) and bottom boundaries were considered as insulated conditions (i.e., zero thermal flux, or equivalently $\partial T/\partial x_i = 0$) due to that the tank was wrapped by a layer of insulation material. The GeoPerformX pipe was between the soil medium and the heater which had a constant volumetric heat flux of **0.521** W/cm^3.

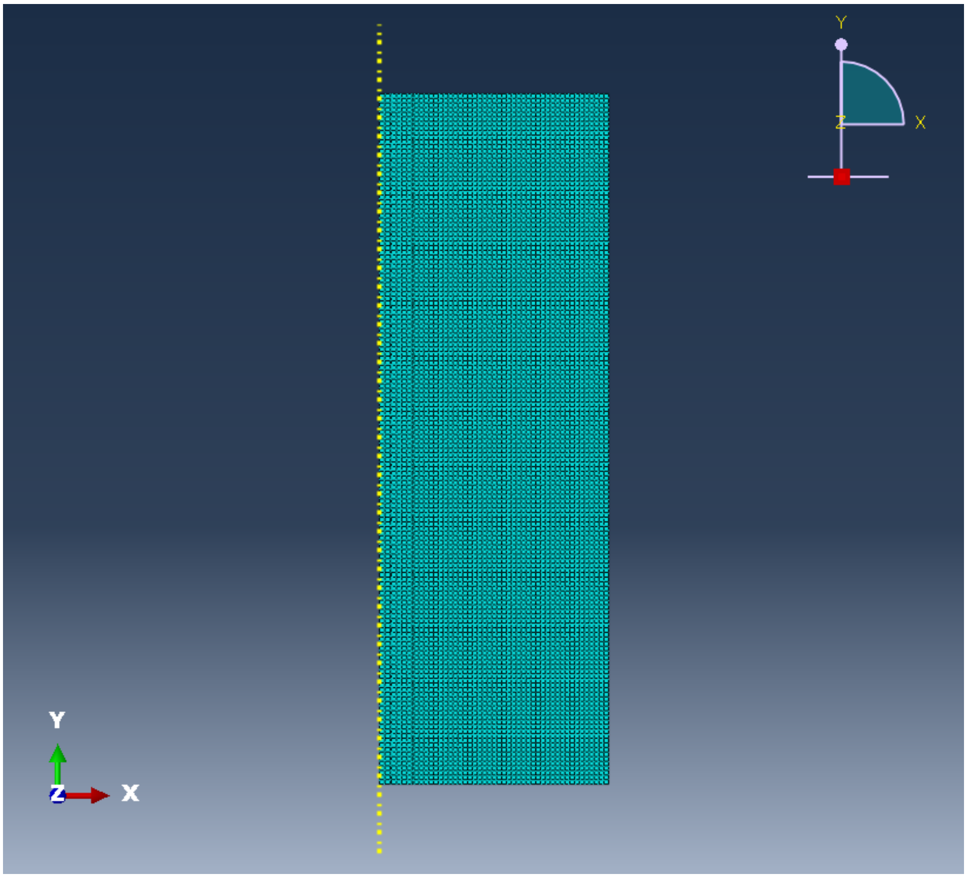

Figure 5.8 Axisymmetric finite element mesh

Numerical simulations were run by assigning the thermal properties to the corresponding materials listed in Table 5.1. Figure 5.9 shows the temperature distribution in the system at the end of the bench scale test when a steady state was achieved.

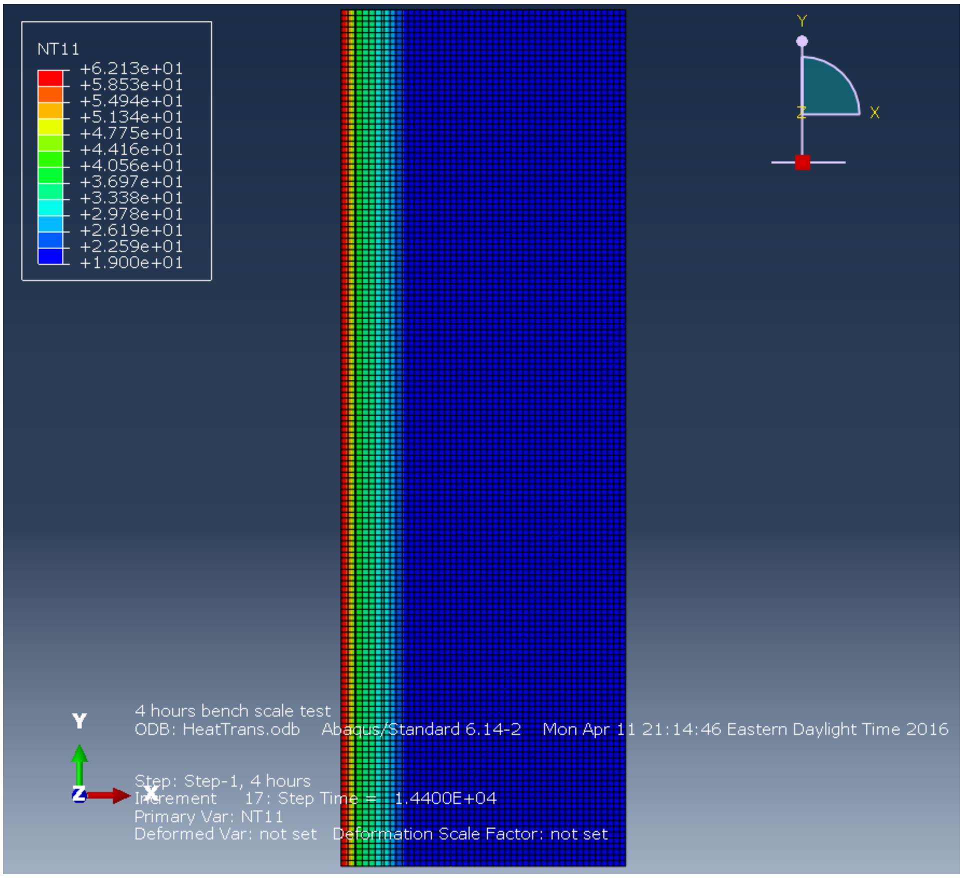

Figure 5.9 Simulated temperature distribution

Table 5.2 and Figure 5.10 compare the temperatures at different locations in soil measured in the bench scale tests, as well as those obtained from numerical simulations. One observes that the simulation generally reproduces the temperature variation with radial distance at the system's steady state. However, the calculated temperature at Point A, which is just outside the aluminum core pipe is higher than that measured in all three onsite tests. This discrepancy can be attributed to the differences in the thermal conductivities of fiber-enhanced grouts tested in the lab and those produced at the site of bench scale tests. When producing grouts on-site, no vacuum was applied to remove air trapped in the composite grout, which was expected to yield lower thermal conductivity than 1.954 W/m·K for the laboratory made composite grout with vacuum applied. Additional laboratory test results summarized in Table 5.3 clearly show that the thermal conductivity of grouts without applying vacuum was approximately 20% lower than that of vacuumed grouts.

As for the temperatures at Points ***B*** to ***E***, the values of temperature obtained from models were lower than the measured ones. This was attributed to the thermal properties of industrial sand used as soil medium in the tank. The assumed thermal conductivity and specific heat capacity of the industrial sand in simulation might have been different from its actual value. Based on the outcome, it is likely that the assumed values were smaller than the actual ones.

Table 5.2 Measured and simulated temperatures at middle height of tank

Location	***A***	***B***	***C-M***	***D***	***E***
Test-1	28.5	22.6	20.2	19	18.9
Test-2	29	23.3	20.8	19.3	19
Test-3	28.2	22.1	19.9	18.9	18.8
Numerical (1.954W/m·K)	32.3	20.7	19.2	19	19

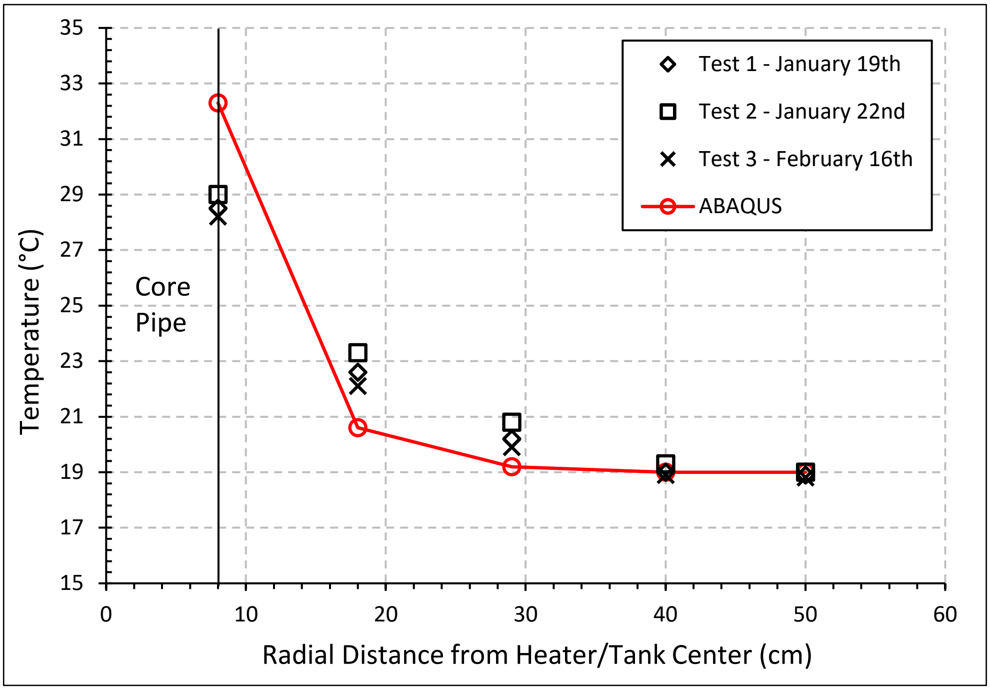

Figure 5.10 Measured and simulated temperature distribution comparison

The temperature difference between the numerical simulation and onsite tests at the edge of borehole/core pipe was likely caused by the heat energy loss during water circulation. Furthermore, a probable air pocket located at edge of the core pipe in the grout could result this temperature drop as well.

Table 5.3 Effect of applying vacuum on grout thermal conductivity

Grout Type		Thermal Conductivity, W/m·°C	
		Before vacuum	After vacuum
Produced in MCR	1.25% AGM94-6mm	**1.552**	**1.841**
Produced in McMaster		**1.540**	**1.954**
Manufacturer recommended	Barotherm Gold, M_S:M_B=8:1	N/A	2.08
Produced in McMaster		**1.662**	**2.013**

To investigate the impact of the thermal conductivity of the grout on the temperature distribution in the media (dry sand), three different grout TC values were used to run the numerical simulations. They were the baseline grout TC value (0.919W/m·K), fiber enhanced grout TC value without vacuum (1.552W/m·K) and that with vacuum (1.954W/m·K). The results are given in Table 5.4 and Figure 5.11.

Table 5.4 Simulated temperatures for different grout thermal conductivities

Location	***A***	***B***	***C-M***	***D***	***E***
Grout TC=1.954W/m·K	32.3	20.7	19.2	19	19
Grout TC=1.552W/m·K	31.1	19.9	19.1	19	19
Grout TC=0.919W/m·K	30.3	19.2	19	19	19

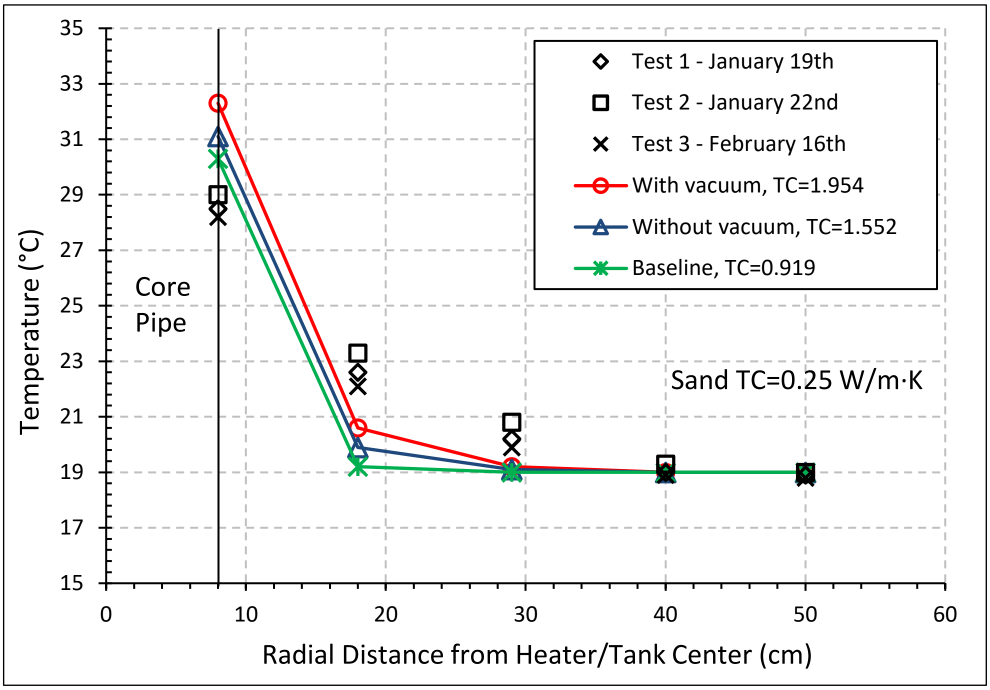

Figure 5.11 Effect of grout thermal conductivity on simulated temperature distribution

One observes that the temperature at the edge of the borehole, Point A, dropped as well as the temperatures in sand (media) when the grout thermal conductivity decreased.

Per Tarnawski and his colleagues (2009), the thermal conductivity of sand varies with its porosity. They tested several types of sand among which a type of quartz sand, Ottawa C-190, had similar particle size distribution compared with the sand used in this study. With repeated test results, the thermal conductivity of this quartz sand at different porosities under 25°C are given in Table 5.5.

Table 5.5 Thermal conductivity of quartz sand at different porosities

Under Temperature @ 25°C			
Porosity, ***n***	0.40	0.36	0.32
Thermal Conductivity, W/m·K	0.250	0.285	0.332

The simulation results by using the sand thermal conductivity values in Table 5.5 are shown in Figure 5.12. Temperatures at Point ***B*** and Point ***C-M*** increased as sand porosity decreased, i.e. denser sand has better heat transfer effect, while at Point ***D*** and Point ***E***, no obvious difference is noted. Per the results, it was highly likely that the dry sand used in MCR bench scale tests had a thermal conductivity ranging from 0.285 to 0.332 W/m·K.

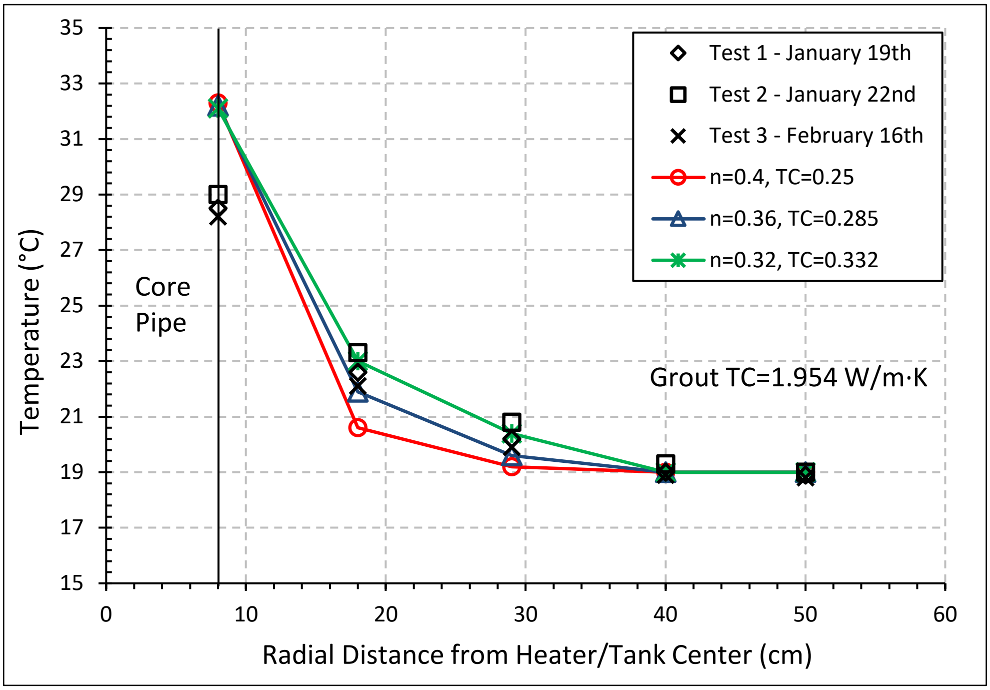

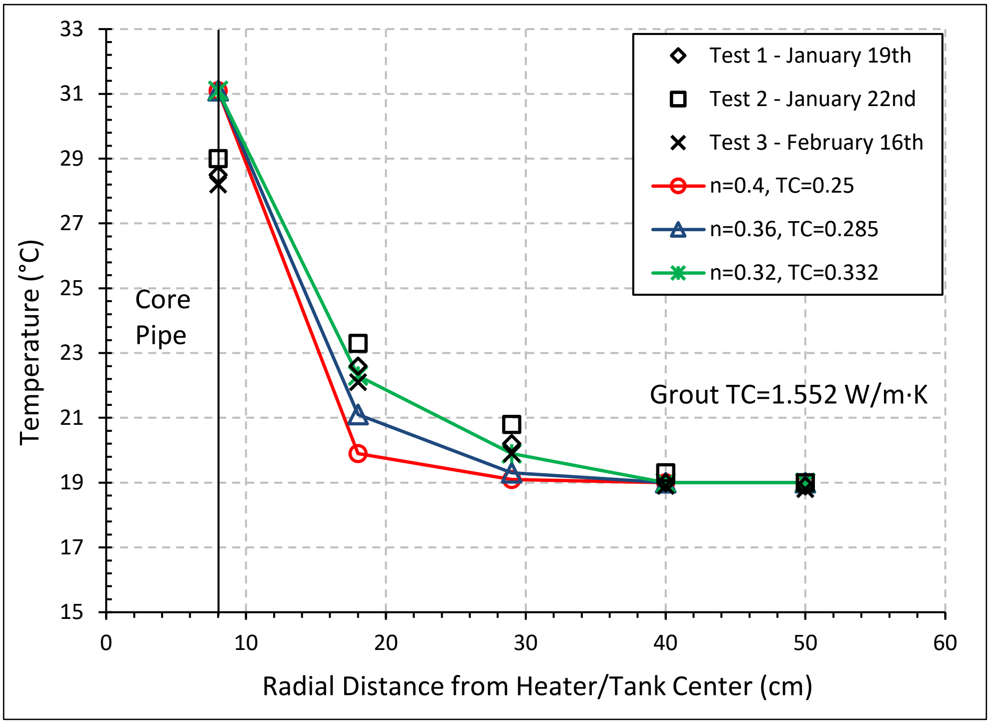

Figure 5.12 Effect of sand porosity on simulated temperature distribution

It was assumed that no interface resistance in this heat transfer model to simplify the simulation as well as due to the unavailability of interfacial heat transfer coefficient, h_{int}, for this experiment. To demonstrate the impact of such interface resistance, one interfacial heat transfer coefficient, h_{int}=42 W/m^{2}·°C, for interface between aluminum alloy and sand mold according to Kubo and Pehlke (1985) was applied on the interface between grout and aluminum pipe, as well as aluminum pipe and sand for this experiment in ABAQUS. The temperatures at the edge of aluminum core pipe, Point A, with and without considering the interface resistance are shown in Table 5.6.

Table 5.6 Temperatures at outside edge of aluminum pipe

Temperature, °C	Ideal contact	Considering interface resistance
Grout TC=1.954W/m·K	32.3	27.3
Grout TC=1.552W/m·K	31.1	26.9
Grout TC=0.919W/m·K	30.3	25.8

Per the simulation results, temperature at outside of aluminum pipe decreased obviously when the interface resistance on both sides of the aluminum pipe was considered.

CHAPTER 6 CONCLUSIONS AND FUTURE WORK

6.1 Summary

This study intended to explore the thermal properties of bentonite-based grout enhanced by adding carbon fibers and the feasibility to practical application in GHPS industry. Through a series of laboratory tests, the thermal properties of bentonite-based grouts enhanced by different types and various fractions of carbon fibers were measured to find fiber-grout mixture that are most efficient and low cost. The selected fiber added grout was next used in bench scale tests to investigate its effectiveness in these small-scale models. Numerical simulations were performed for a parametric study on the sensitivity of temperature distribution with respect to different parameters. The findings obtained from this research are summarized as follows.

6.1.1 Conclusions from laboratory test results

1. Adding higher volumetric percentage and longer carbon fibers can increase the thermal conductivity of bentonite-based grout efficiently.

2. The longest AGM94-6mm carbon fiber (PAN) has the best enhancement effect on bentonite-based grout thermal performance among all the five fiber types of fiber examined in this study.

3. Shorter carbon fibers have limited effect in thermal conductivity enhancement of bentonite-based grout but perform more consistently compared with longer fibers.

4. Under the same volumetric percentage, the greater the carbon fiber aspect ratio is, the higher the composite grout thermal conductivity will be.

5. Carbon fibres made from polyacrylonitrile (PAN) have better enhancement effect than those made from petroleum pitch. The Pitch-based AGM95-6mm carbon fiber has the same effect as the PAN-based AGM94-3mm fiber, both have slightly poor thermal enhancement effect than the PAN-based AGM94-6mm fiber, even though Pitch-based AGM95-6mm fiber has slightly higher carbon content.

6. The strength of carbon fiber may also have some influence on the thermal enhancement effect. Long fibers with higher strength are preferable, since low strength fibers tend to break in the mixing process, resulting in relatively poor enhancement to thermal conductivity.

7. The specific heat capacity of fiber enhanced composite grout increases when the temperature goes up. However, addition of carbon fibers only has marginal effect on the heat capacity of composite grouts, and no obvious variation trend is observed as the volumetric fraction of carbon fiber is increased.

6.1.2 Conclusions from bench scale experiment and numerical simulations

The temperature distribution pattern computed by FEM simulation using ABAQUS reasonably reproduces the MCR bench scale experimental results. This verifies the thermal performance of carbon fiber added bentonite-based grout achieved from the laboratory tests.

The difference between measured and computed temperature values also reflects the effect of vacuum step during the composite grout producing process as well as the accuracy of parameter values in simulation. The interfacial heat transfer resistance also impacts simulation results.

Specification of dry sand, the soil medium in the bench scale tests, also has influence on temperature distribution. Under the same conditions, sand with a lower porosity (or higher density) has higher thermal conductivity, which results in a higher temperature in the soil medium.

6.2 Future work

While the effectiveness of thermal conductivity enhancement of carbon fibers for bentonite-based grout has been proven in this study, other properties of carbon-fiber treated bentonite-based grout should still be investigated to promote its application in engineering practice.

It should be noted that the conclusions as summarized above are based on test results on limited number of variables. The following work is necessary for future investigations:

1. The effect of different types of carbon fibers on the viscosity, workability, flowability and pumpability of bentonite-based grout should be investigated. The viscosity and pumpability are especially important for GHPS using deep boreholes.

2. Different mixing and producing processes can largely affect the thermal conductivity of carbon fiber added bentonite-based grout. Applying vacuum to remove trapped air is essential in determining the theoretical thermal conductivity value of composite grout. However, this step is not commonly used in engineering application. Future investigation should try to find a solution for this problem.

3. The drying-wetting process may have significant effect on the thermal conductivity of bentonite-based grouts, which in turn affects the seasonal variation of a GHPS performance. How the thermal properties change in a carbon fiber added composite grout is affected by the drying-wetting process should also

be investigated.

4. Life-cycle cost analysis (LCCA) is necessary to promote the application of carbon fiber enhanced grouts in GHPS. Optimization of the grouts should take into account both short-term cost relating to material, workability, and long-term cost.

5. The specific heat capacity test in this study used DSC method of which the size of sample hermetic container was constrained at 6mm diameter. This will limit the length of carbon fiber as additive if longer fiber is investigated. Further work is necessary to explore new reliable experimental method to measure the specific heat capacity of composite grout.

6. The current numerical model is only capable to do simple heat transfer analysis and/or semi-coupled analysis. Future study on computational simulation should be focused on fully-coupled hydro-mechanical-thermal model for considering more factors such as underground water, stress, and interface thermal resistance.

7. Influence of some material properties and environmental conditions on the thermal performance of developed carbon fiber added composite grout is still unclear. Future research should consider more variables such as different add-in material other than industrial sand to expand the potential application.

REFERENCES

Acari, Y., Ueda, A., & Nacal, S. (1991). Thermal Conductivity of a Polyethylene Filled with Disoriented Short-Cut Carbon Fibers. *Journal of Applied Polymer Science*, *43*, 1117–1124.

Alrtimi, A. A., Rouainia, M., & Manning, D. C. (2013). Thermal enhancement of PFA-based grout for geothermal heat exchangers. *Applied Thermal Engineering*, *54*(2), 559–564.

Beier, R. (2014). Transient heat transfer in a U-tube borehole heat exchanger. *Applied Thermal Engineering*, *62*(1), 256–266.

Börgesson, L., Fredrikson, A., Johannesson (1994). Heat conductivity of buffer materials. SKB TR-94-29.

Borinaga-Treviño, R., Pascual-Muñoz, P., Castro-Fresno, D., & Del Coz-Díaz, J. J. (2013). Study of different grouting materials used in vertical geothermal closed-loop heat exchangers. *Applied Thermal Engineering*, *50*(1), 159–167.

Cadge, D., Wang, J. H., Bie, J., Sun, X., Bai, R., & Gong, P. (2006). *COUPLED THERMAL-MOISTURE-STRESS ANALYSIS FOR ELECTRONIC PACKAGES*.

Chiasson, A. D. (1999). *Advances in Modeling of Ground-Source Heat Pump Systems*.

Clauser, C., & Huenges, E. (2013). Rock Physics & Phase Relations: A Handbook of Physical Constants. Thermal Conductivity of Rocks and Minerals. *American Geophysical Union*, *3*(Thermal Conductivity of Rocks and Minerals), 105–126.

Delaleux, F., Py, X., Olives, R., & Dominguez, A. (2012). Enhancement of geothermal borehole heat exchangers performances by improvement of bentonite grouts conductivity. *Applied Thermal Engineering*, *33–34*(1), 92–99.

Demain, A., & Issi, J.-P. (1993). The Effect of Fiber Concentration on the Thermal Conductivity of a Polycarbonate/Pitch-Based Carbon Fiber Composite. *Journal of Composite Materials*, *27*(7), 668–683.

Desmedt, J., Van Bael, J., Hoes, H., & Robeyn, N. (2012). Experimental performance of borehole heat exchangers and grouting materials for ground source heat pumps. *International Journal of Energy Research*, *36*(August 2011), 1238–1246.

Eppelbaum, L., Kutasov, I., & Pilchin, A. (2014). *Applied Geothermics*. *Applied Geothermics*.

Fujii, H., Komaniwa, Y., Nomoto, T., & Chou, N. (2011). Reduction of Thermal Resistance of Ground Heat Exchangers using Large Grain Size Materials. *GRC*

Transactions, *35*, 1095–1100.

Horai, K., & Simmons, G. (1969). Thermal conductivity of rock-forming minerals. *Earth and Planetary Science Letters*, *6*(5), 359–368.

Hong, C. P. (2004). Computer Modelling of Heat and Fluid Flow in Materials Processing. https://doi.org/10.1201/9781420057010.

Incropera, F. P., DeWitt, D. P., Bergman, T. L., & Lavine, A. S. (2007). *Fundamentals of Heat and Mass Transfer*. (F. P. Incropera & F. P. F. O. H. A. M. T. Incropera, Eds.), *Water* (Vol. 6th). John Wiley & Sons.

Kiyohashi, H., Sasaki, S., & Masuda, H. (2003). Effective thermal conductivity of silica sand bed as a filling material for crevices around radioactive- waste canisters. *High Temperatures-High Pressures*, *35/36*(2), 179–192.

Kubo, K., Pehlke, D. (1985). *Metall. Trans. 16B*, 359-366.

Lee, C., Lee, K., Choi, H., & Choi, H. P. (2010). Characteristics of thermally-enhanced bentonite grouts for geothermal heat exchanger in South Korea. *Science China Technological Sciences*, *53*(1), 123–128.

Leung, C., Holton, D., & Thetford, R. (2014). *Review of the current status of work on* *enhanced bentonite buffer materials* (Vol. 1).

Lienhard, J. H. (2010). Heat Transfer. *Journal of Heat Transfer*, *82*(1), 198.

Mands, E., & Sanner, B. (n.d.). In-situ-determination of underground thermal parameters. *Technology*, 1–10.

Miller, C. J., Asce, M., & Rifai, S. (2004). Fiber Reinforcement for Waste Containment Soil Liners. *Journal of Environmental Engineering*, *130*(8), 891–895.

Naito, K., Yang, J.-M., Xu, Y., & Kagawa, Y. (2010). Enhancing the thermal conductivity of polyacrylonitrile- and pitch-based carbon fibers by grafting carbon nanotubes on them. *Carbon*, *48*, 1849–1857.

Niekamp, A., Unklesbay, K., Unklesbay, N., & Ellersieck, M. (1984). Thermal Properties of Bentonite-Water Dispersions Used for Modeling Foods. *Journal of Food Science*, *49*(1), 28–31.

Ojas, W. (1997). *AN EXPERIMENTAL AND NUMERICAL STUDY OF THE THERMAL PERFORMANCE OF A BRIDGE DECK DE-ICING SYSTEM*. Oklahoma State University.

RETScreen ® International. (2004). *GROUND-SOURCE HEAT PUMP PROJECT*

ANALYSIS CHAPTER.

Robertson, E. C. (1988). Thermal Properties of Rocks. *US Department of the Interior: Geological Survey*, 88–441.

Rozanski, A. (2016). On the prediction of the thermal conductivity of saturated clayey soils: Effect of the specific surface area. *Acta Geodynamica et Geomaterialia*, *13*(4), 339–349.

Rühaak, W., & Sass, I. (2013). APPLIED THERMO-HYDRO-MECHANICAL COUPLED MODELING OF GEOTHERMAL PROSPECTION IN THE NORTHERN UPPER RHINE GRABEN. In *PROCEEDINGS*. Stanford, California: Stanford University.

Sanner, B. (2003). Current status of ground source heat pumps in Europe. *Proc. of the 9th Int. Conf. on Thermal Energy Storage FUTURESTOCK*, 695–703.

Simms, R. B., Haslam, S. R., & Craig, J. R. (2014). Impact of soil heterogeneity on the functioning of horizontal ground heat exchangers. *Geothermics*, *50*, 35–43.

Smits, K., Sakaki, T., Limsuwat, A., & Illangasekare, T. H. (2009). Thermal conductivity of sands under varying moisture, drainage/wetting, and porosity conditions-applications in near-surface soil moisture distribution analysis. *AGU*

Hydrology Days, *30*(4), 57–65.

Spitler, J. D., Qing, G., Li, M., Yan, J., & Guang, Q. (2006). PRACTICE AND TASK DEVELOPING UNDERGROUND THERMAL ENERGY STORAGE IN CHINA. *Energy*, 1–8.

Stefaniuk, D., Różański, A., & Łydżba, D. (2016). Recovery of microstructure properties: random variability of soil solid thermal conductivity. *Studia Geotechnica et Mechanica*, *38*(1).

Tarnawski, V. R., Momose, T., & Leong, W. H. (2011). Thermal conductivity of standard sands II. Saturated conditions. *International Journal of Thermophysics*, *32*(5), 984–1005.

Tarnawski, V. R., Momose, T., Leong, W. H., Bovesecchi, G., & Coppa, P. (2009). Thermal conductivity of standard sands. Part I. dry-state conditions. *International Journal of Thermophysics*, *30*(3), 949–968.

Tiedje, E. W., & Guo, P. (2013). Thermal Conductivity of Bentonite Grout Containing Graphite or Chopped Carbon Fibers. *Journal of Materials in Civil Engineering*.

Tiedje, E. W., & Guo, P. (2014). Modeling the influence of particulate geometry on the thermal conductivity of composites. *Journal of Materials Science*, *49*(16), 5586–5597.

Yeung, K. D. (1996). *Enhancements to a ground loop heat exchanger design program*. *Oklahoma State University*.

Zalba, B. (2003). Review on thermal energy storage with phase change: materials, heat transfer analysis and applications. *Applied Thermal Engineering*, *23*(3), 251–283.

Zheng, Z., Wang, W., & Ji, C. (2011). A study on the thermal performance of vertical U-tube ground heat exchangers. *Energy Procedia*, *12*, 906–914.